MARTIN MARIETTA ENERGY SYSTEMS LIBRARIES

3 4456 0348254 0

ORNL/TM-11492

ornl

OAK RIDGE
NATIONAL
LABORATORY

MARTIN MARIETTA

Thermal Energy Storage Technical Progress Report April 1988–March 1989

J. J. Tomlinson
R. J. Kedl

OAK RIDGE NATIONAL LABORATORY
CENTRAL RESEARCH LIBRARY
CIRCULATION SECTION
4500N ROOM 175
LIBRARY LOAN COPY
DO NOT TRANSFER TO ANOTHER PERSON
If you wish someone else to see this report, send in name with report and the library will arrange a loan.

OPERATED BY
MARTIN MARIETTA ENERGY SYSTEMS, INC.
FOR THE UNITED STATES
DEPARTMENT OF ENERGY

This report has been reproduced directly from the best available copy.

Available to DOE and DOE contractors from the Office of Scientific and Technical Information, P.O. Box 62, Oak Ridge, TN 37831; prices available from (615) 576-8401, FTS 626-8401.

Available to the public from the National Technical Information Service, U.S. Department of Commerce, 5285 Port Royal Rd., Springfield, VA 22161.
NTIS price codes—Printed Copy: A05 Microfiche A01

This report was prepared as an account of work sponsored by an agency of the United States Government. Neither the United States Government nor any agency thereof, nor any of their employees, makes any warranty, express or implied, or assumes any legal liability or responsibility for the accuracy, completeness, or usefulness of any information, apparatus, product, or process disclosed, or represents that its use would not infringe privately owned rights. Reference herein to any specific commercial product, process, or service by trade name, trademark, manufacturer, or otherwise, does not necessarily constitute or imply its endorsement, recommendation, or favoring by the United States Government or any agency thereof. The views and opinions of authors expressed herein do not necessarily state or reflect those of the United States Government or any agency thereof.

ORNL/TM-11492
Dist. Category UC-202

ENGINEERING TECHNOLOGY DIVISION

THERMAL ENERGY STORAGE TECHNICAL PROGRESS REPORT APRIL 1988-MARCH 1989

J. J. Tomlinson
R. J. Kedl

Date Published - March 1990

Prepared by the
OAK RIDGE NATIONAL LABORATORY
Oak Ridge, Tennessee 37831
operated by
MARTIN MARIETTA ENERGY SYSTEMS, INC.
for the
U.S. DEPARTMENT OF ENERGY
under contract DE-AC05-84OR21400

MARTIN MARIETTA ENERGY SYSTEMS LIBRARIES
3 4456 0348254 0

CONTENTS

	Page
LIST OF FIGURES	v
LIST OF TABLES	vii
ABSTRACT	1
1. PROGRAM OVERVIEW	1
1.1 DIURNAL TES	3
1.2 INDUSTRIAL TES	7
2. TECHNICAL PROGRAM - DIURNAL THERMAL ENERGY STORAGE	9
2.1 DEVELOPMENT OF ICE SELF-RELEASE MECHANISMS	9
2.2 EVAPORATIVE HEAT TRANSFER	11
2.3 EFFECT OF DOPANTS ON SOLID-STATE PCMs	18
2.4 LIQUID-LIQUID SYSTEMS FOR TES	23
2.5 COMPUTER MODELING OF BUILDING MATERIALS CONTAINING PCMs	30
2.6 DEVELOPMENT OF COMPLEX-COMPOUND CHILL STORAGE SYSTEM	34
2.7 DIRECT CONTACT ICE STORAGE SYSTEM DEVELOPMENT	44
2.8 INCORPORATION OF PCMs INTO BUILDING CONSTRUCTION MATERIALS	46
2.9 PCM WALLBOARD FABRICATION AND TESTING	52
3. TECHNICAL PROGRAM - INDUSTRIAL THERMAL ENERGY STORAGE	60
3.1 PACKED-BED TES MODEL FOR INDUSTRIAL APPLICATIONS	60
3.2 TES OPTIMIZATION FOR PERIODIC BRICK PLANT	68
4. CONCLUSIONS	77
REFERENCES	79

LIST OF FIGURES

Page

Fig. 1a. Diurnal TES subprogram. 4

Fig. 1b. Industrial TES subprogram. 4

Fig. 2. Two-sided ice formation fixture. 10

Fig. 3. Annular test fixture with inside solution column and outside thermal guard. 10

Fig. 4. Schematic layout of packed-bed evaporator test facility. 13

Fig. 5. Heat transfer probe and details. 14

Fig. 6. Forced convection validation of heat transfer measurement system. . . 15

Fig. 7. Variation of boiling results with ΔT^* and comparison with present correlation; 1.59 cm spheres in cluster. 19

Fig. 8. Variation of boiling results with ΔT^* and comparison with present correlation; 2.54 cm spheres in cluster. 20

Fig. 9. Thermal expansions in pentaglycerine (PG) and pentaerythritol (PE) in a- and c-directions. 24

Fig. 10. Heats of mixing for triethylamine-urea-water; $x^i_u = 0.077$. 28

Fig. 11. Heats of mixing for triethylamine-urea-water; $x^i_u = 0.1$. 29

Fig. 12. Heats of mixing for diethylene glycol diethyl ether (1)-NaCl-water; $x^i_{NaCl} = 0.0113$. 31

Fig. 13. Adsorption uptake curve for CC480 35

Fig. 14. Reactivity of CC180. 38

Fig. 15. Cool storage concept using compressor. 40

Fig. 16. Discharge of complex compound chill storage system. 41

Fig. 17. Refrigeration loop with complex compound TES system. 42

Fig. 18. Direct contact system flow schematic. 45

Page

Fig. 19. DSC plot for n-Octadecane. 48

Fig. 20. Variation of flexural strength with concentration for three thicknesses. 51

Fig. 21. Immersing wallboard in wax. 53

Fig. 22. Wax absorbed by wallboard as function of immersion time. 55

Fig. 23. Fixture for measuring thermal conductivity and developing thermal transient data. 58

Fig. 24. Thermal conductivity as a function of temperature for gypsum-wax specimens. 59

Fig. 25. Transient response over a complete cycle (charge, dwell, and discharge) for a packed bed utilizing five different PCMs; mass flowrate = 0.5 kg/s-m^2. 62

Fig. 26. Temperature-axial position profiles for a packed bed utilizing five families of PCM; charge period. 63

Fig. 27. Temperature-axial position profiles for a packed bed utilizing five families of PCM; discharge period. 64

Fig. 28. Comparison of the transient performance for the packed bed: (i) utilizing five PCM sets, (ii) utilizing five PCM sets with wall effect neglected, and (iii) utilizing one PCM. IN = inlet fluid temperature; OUT = outlet fluid temperature. 65

Fig. 29. Transient performance of the packed bed TES unit utilizing one PCM family; T_{ph} = 1,000K. 66

Fig. 30. Transient performance of the packed bed TES unit utilizing five PCM families; T_{ph} = 1,000K, 900K, 800K, 700K, and 500K. 67

Fig. 31. Example brick plant. 70

Fig. 32. Example plant schedule. 71

Fig. 33. Dynamic storage optimization. 75

LIST OF TABLES

Page

Table 1. Thermal data on doped pentaglycerine samples. 22

Table 2. Aqueous systems with glycol mixtures. 26

Table 3. Weight loss of 1/2-in. wallboard aged 1, 2, and 3 months in air at 100°F. 50

THERMAL ENERGY STORAGE TECHNICAL PROGRESS REPORT APRIL 1988-MARCH 1989

J. J. Tomlinson
R. J. Kedl

ABSTRACT

The Department of Energy (DOE) is charged with supporting development of technologies that improve the energy and environmental posture of the nation in terms of increased energy efficiency and fuel switching strategies that emphasize greater reliance on indigenous energy resources. As an enabling technique for utilization of renewable energy resources and for improvement of utility load factors, thermal energy storage (TES) can play a vital role. Progress in the development of TES technologies under Oak Ridge National Laboratory's (ORNL) TES Program for the period April 1988 to March 1989 is reported. Each of the projects in the diurnal and industrial TES subprogram is discussed, and their integrated role in support of major application areas is defined.

---

1. PROGRAM OVERVIEW

Thermal energy storage covers a wide range of technologies that allows an energy supply to be coupled to a heating or cooling demand. In many cases, neither is the demand for heating or cooling constant (e.g., building space conditioning or an industrial drying operation) nor is the energy supply constant. In such cases of "temporal mismatch," TES acts as a buffer storing energy when the supply exceeds the demand and supplementing the energy supply (by discharging the TES system) when the demand is greater. In this way, TES effectively couples the energy supply with demand. Major economic benefits can be derived from applying TES to heating or cooling systems. These benefits include: (1) heating/cooling equipment downsizing, (2) expansion of heating/cooling capacity through the addition of TES, (3) load management, (4) industrial waste heat utilization, and (5) increased use of renewable energy sources.

Equipment downsizing. In many applications such as building space conditioning, the demand for heating or cooling may vary greatly with time. Without TES, the heating/cooling equipment must be sized to meet the peak demand. With TES acting as a "thermal flywheel" this peak demand can be met with a smaller, less costly energy supply system.

Capacity expansion. As an alternative to downsizing heating/cooling equipment, TES applied to existing equipment can increase its peak capacity thereby allowing a heating/cooling system that was expressly designed for one load to meet a still larger load.

Electric load management. Thermal energy storage provides the capability to tailor, intentionally, the pattern of electricity use to meet a given thermal load. This capability is beneficial to electric power generation where, through TES, excess baseload capacity can be used at times that do not coincide with the demand for thermal energy. Electric load management improves the capacity factor and overall efficiency of the electric utility by reducing the peak electrical demand.

Waste heat utilization. In many industries, heat is required in a process that does not coincide with the availability of waste heat. A TES system provides a means for capturing waste heat for use in a later process. The result is an overall reduction in the energy requirements of the industry.

Use of renewable energy. Examples of this application include utilization of solar energy for nighttime heating or, on a longer term, the use of winter chill for cooling in summer.

Implementation of TES rests on the availability of a suitable TES medium and a system coupled to an energy source and load for charging and discharging. Thermal storage occurs through a change in thermodynamic state of a material; consequently, every material can be considered as having a TES capability. Yet, relatively few materials currently meet the cost, performance, safety, physical, and/or chemical constraints required for implementation as a working TES medium in specific applications. In addition, there are significant technical issues concerned with TES media containment, effective heat exchange between TES media and

working fluid(s), and cost-effective means for incorporation of TES systems into these applications as well. In support of its historic mission, the DOE has continued to address technical issues with TES media and systems with a goal of advancing TES technologies to the point of adoption by the private sector. The DOE TES Program is organized into three application areas: diurnal, industrial, and seasonal applications. Oak Ridge National Laboratory is the principal research laboratory for two of these areas: diurnal and industrial TES technology development, and accepts a role of field management in those areas for DOE's Office of Energy Storage and Distribution. This report presents the accomplishments and status of in-house and subcontracted projects active under ORNL's TES program during the 1-year period ending March 31, 1989.

1.1 Diurnal TES

The application targets for the diurnal TES subprogram are development of TES for passive solar applications and for off-peak building heating and cooling systems. Projects have been classified into the following technical areas:

1. Heat transfer enhancement
2. System development
3. System/component studies
4. Mathematical modeling
5. Media (i.e., materials) development

These major technical areas along with projects currently underway in each of these areas are shown in Fig. 1a. Note that each project supports one of two application targets.

Heat transfer enhancement

Heat transfer is a critical issue in all TES applications because it limits the rate at which thermal energy can be provided to or withdrawn from a source and delivered to an end use. In latent heat storage applications, fouling due to solids freezing to a heat exchanger surface

Fig. 1a. Diurnal TES subprogram.

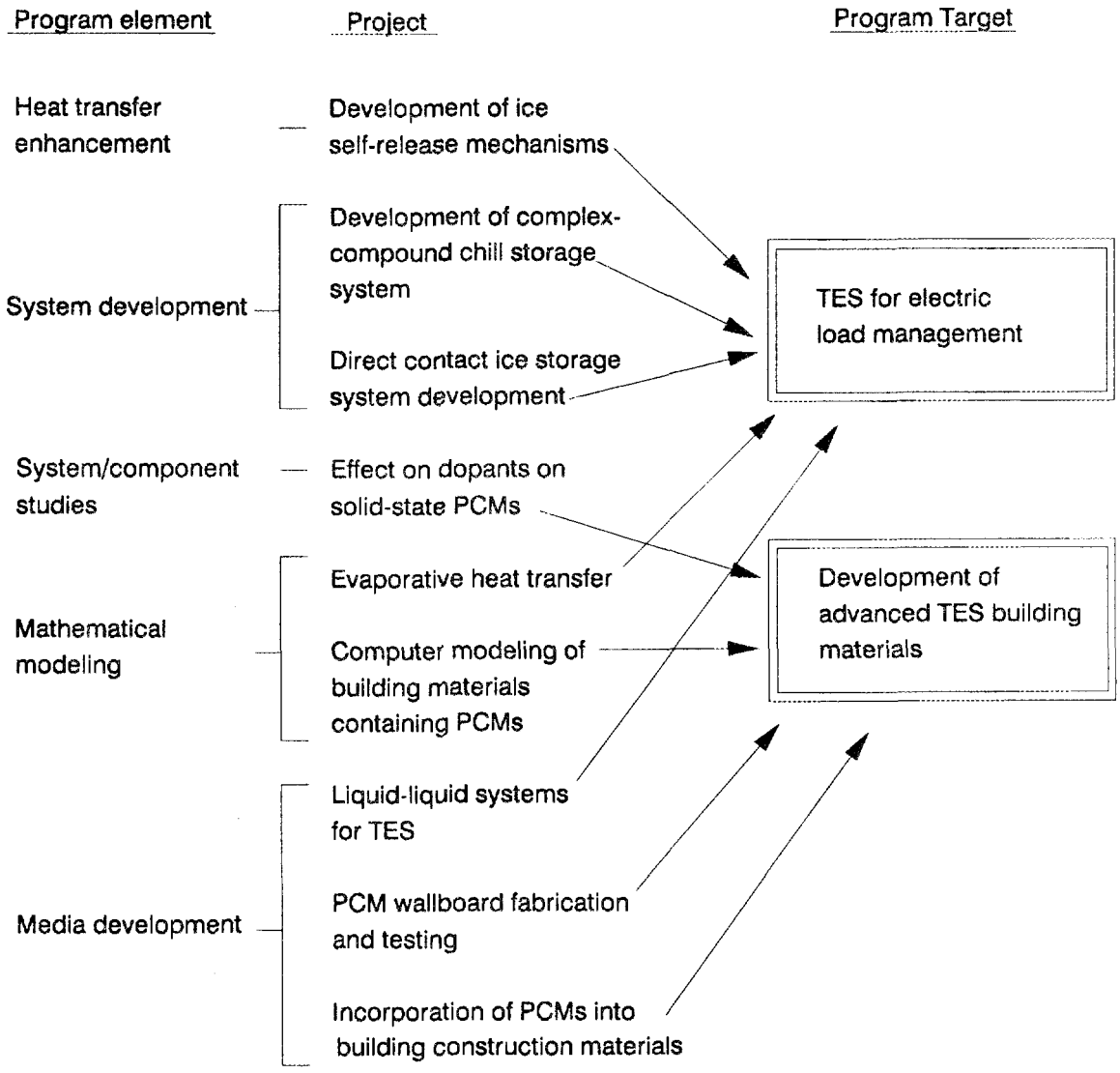

Fig. 1b. Industrial TES subprogram.

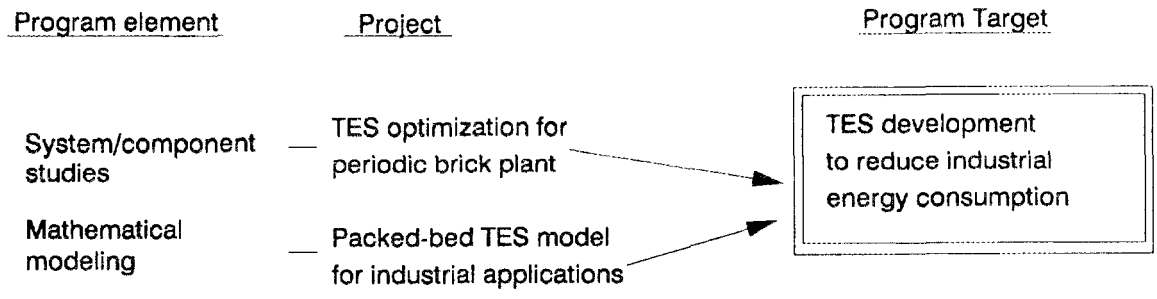

during a charging cycle (as in the case of cool storage) or discharging cycle (as in the case of heat storage) is frequently the limiting heat transfer mechanism. Conventional methods to accommodate this problem are provisions for large surface heat exchangers or systems that mechanically or thermally clean the heat exchange surface. Either technique results in increased costs.

In ice storage systems wherein ice is formed for later building cooling, work was continued to address the heat transfer issue. The first was a study of methods whereby an evaporator surface used to form ice can be made "self-cleaning," i.e., the ice that is formed floats or falls away from the surface thereby continuously refreshing the surface. This project showed, that with suitable water additives and evaporator surfaces, ice can be made to release spontaneously from the substrate. The process appears to be very sensitive to the temperature difference between the ice being formed and the substrate and ceases altogether when this temperature difference is larger than 2°C.

System development

System development is an area covering two projects in the cool storage temperature range. In one project, the principle of chemisorption is being used to develop a chill storage system for low temperature refrigeration applications. Although TES systems based on sorption are not new, development of a cost-effective system is challenging. A major improvement in heat and mass transfer using a dry bed reactor has put the economics of an ammoniated complex-compound TES system well-within reach. A second project is the development of an advanced direct-contact ice storage system for building cooling. This system is being developed in a size suited for later field testing. The system design is such that oil and water carryover problems that have paralyzed early efforts to exploit the direct contact approach have been resolved through use of a unique compressor technology.

System/component studies

In many cases, particularly with polyalcohols, the solid-solid (solid-state) transition is much more energetic than the solid-liquid phase change and occurs at a temperature far below the melt temperature. The objective of the project under System/component studies is development of organic solid-state phase change materials (PCMs) at selected temperatures. Through the use of dopants to strain the crystal lattice, PCM alloys that undergo solid-solid phase transitions are being tailored for particular temperature applications (e.g., passive solar) with only proportionate decreases in transition energetics. The near-term project objectives are to understand the molecular structure of the host and interactions between the host and dopant species during the solid-state transition.

Mathematical modeling

Solutions to most of the interesting problems involving energy storage through phase change are found only through mathematical modeling using iterative techniques. There has been significant progress during the reporting period in two efforts that model a phase change system. The objective of the first effort is development of a thermodynamic description of a packed bed of PCM immersed in a boiling heat transfer fluid. An excellent heat transfer correlation between a heated packed bed and an evaporating heat transfer fluid was developed and experimentally verified. The verified model will be used for technical evaluation of storage heat pump systems with PCMs used as evaporators.

A second modeling project is underway to provide guidance in current research efforts to incorporate PCMs into building materials such as wallboard. This project consists of development of a mathematical model of PCMs dispersed throughout a sensible heat matrix. The model, developed for use on a microcomputer, will be validated experimentally and later used to quantify benefits of a wallboard containing a PCM.

Media development

As storage materials, PCMs are favored over sensible heat storage media from the standpoint of smaller size, less weight and the ability to store and deliver heat over a small temperature interval. Thus development of TES media in which one or more components undergo a phase change remained a central element of the ORNL TES program. The project to examine latent heat storage in multicomponent liquid systems that exhibit large miscibility changes over small temperature ranges was continued. The behavior of ternary systems used to adjust this temperature range according to an intended application was identified and several third components suited for use in glycol systems were identified.

A major target of the ORNL TES program is the development of a gypsum wallboard material containing a PCM. The advantage of this concept is that a significant amount of "thermal mass" can be provided to stud wall construction by using the PCM wallboard. The benefit to the occupant is increased thermal comfort and efficiency improvements in building space conditioning through greater utilization of passive solar energy. Two projects were continued in support of this concept: one is aimed at the development of a PCM wallboard system containing a paraffin as the PCM; the other, an in-house project, evaluated issues connected with incorporation of the PCM into plasterboard through immersion and scale-up of the process to full (4 x 8 ft) size.

1.2 Industrial TES

The scope of the industrial program is shown in Fig. 1b indicating projects that were continued or initiated during the reporting period.

System component/studies

An optimization study was initiated and aimed at determining the "best" (highest return-on-investment [ROI]) high-temperature storage configuration for a two-kiln, single-dryer periodic brick plant. The study takes into account real-time uses for reject heat for which storage is not

required. During the reporting period, a methodology was developed based on use of linear and dynamic programming techniques to determine an optimal TES configuration and operating sequence in the presence of an intermittent heat source and variable heat demand. This methodology is a significant advancement in the design and operation of TES systems. A preliminary study of TES in the simple periodic brick plant was completed; extension of this study to an arbitrary plant is underway.

Mathematical modeling

Work was continued on improvements to a high-temperature packed bed thermal model. The near-term application of this model is to support the design of a high temperature facility for testing TES media; in the longer term the model will be available as a design tool for full-scale industrial TES systems. During the reporting period, capabilities of the model were extended to include a packed bed containing PCMs over a range of melting points, wall effects, and a gas inlet stream with varying mass flow rates, temperatures, and chemical compositions.

2. TECHNICAL PROGRAMS - DIURNAL THERMAL ENERGY STORAGE

2.1 Development of Ice Self-Release Mechanisms

A number of ice-making concepts for summertime peak electric demand reduction are based on the periodic removal of ice from the surface on which it is formed. Commonly, ice is melted off the surface, although it can be removed by other means. In any case, ice removal requires energy, and the efficiency of the ice maker is decreased accordingly. In the past, a number of researchers[1] have investigated the possibility of developing a surface/water (ice) system where the adhesion of ice to the surface is very low. Thus ice can self-release and fall off the surface under the influence of gravity or can float off the surface under the influence of buoyancy. Previous research[2] has identified certain conditions necessary to achieve low adhesion. The surface should be glassy smooth, and it must be hydrophobic or nonwettable by water. It has been found[3] that small concentrations of electrolytes in the water will decrease the adhesion. A commercially acceptable ice self-release system has not yet been developed, but the search continues because the benefits would be considerable.

In one study,[4] the University of Missouri experimentally evaluated a number of ice self-release techniques. One technique involved coating the heat exchange surface with Rilsan and using water containing dissolved electrolytes. This combination resulted in ice repeatedly self-releasing from a submerged evaporator surface.

The University of Missouri was funded by the ORNL TES Program to continue development of this concept. The objectives of this research were to define the physical-chemical mechanisms involved in ice self-release, to address the parametric limits of the self-release process, and to determine the suitability of the concept for application in a large-scale engineered system.

The experimental apparatus for this study consisted of a vertically orientated surface (shown in Fig. 2) on which ice could be formed. The surface was cooled by pumping an antifreeze solution through a heat exchange cavity formed by the two sides of the ice formation

ORNL-DWG 89-4413 ETD

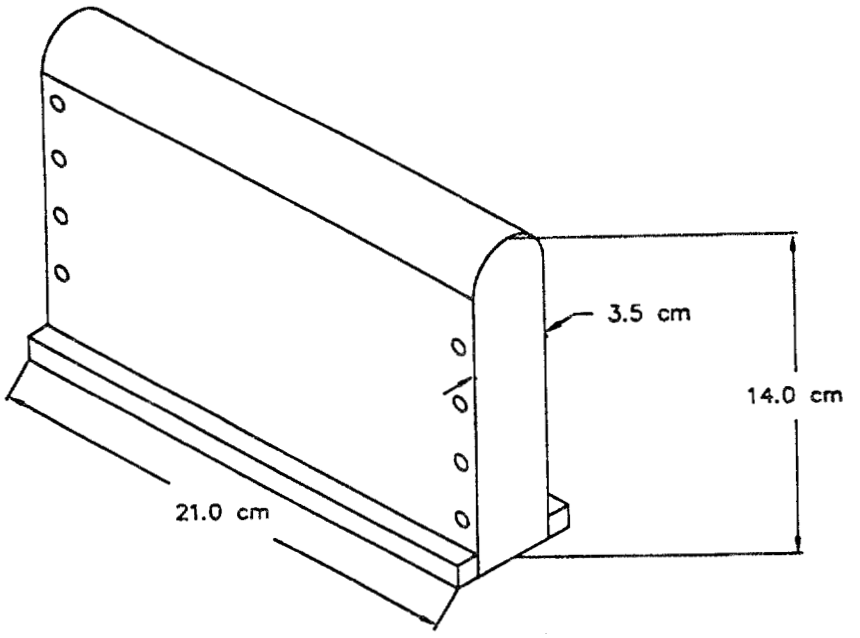

Fig. 2. Two-sided ice formation fixture.

ORNL-DWG 89-4412A ETD

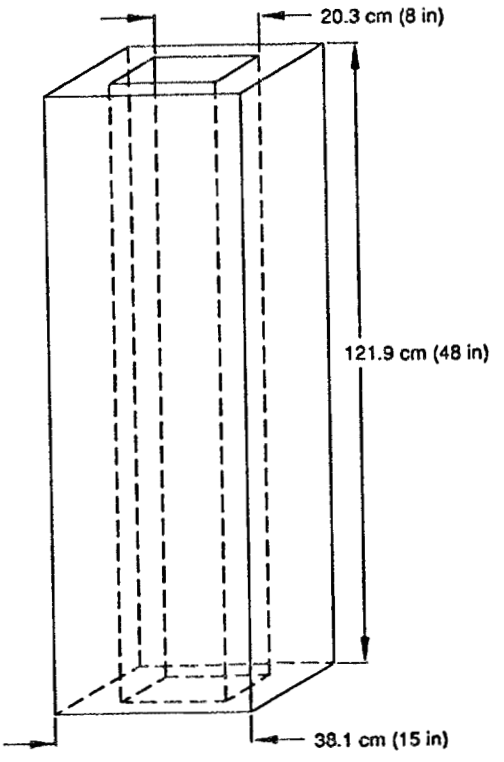

Fig. 3. Annular test fixture with inside solution column and outside thermal guard.

fixture. This fixture was submerged under 4 ft of water in the inner solution column shown in Fig. 3. A cold antifreeze solution was pumped through the outer column to act as thermal insulation.

In this research, it was demonstrated that self-release of ice could be achieved continuously and reliably; however, certain conditions had to be met. The most critical parameter governing the self-release of ice was found to be the temperature difference, ΔT, between the ice formation surface and the freezing point of the solution. This ΔT must be $<2°C$. If the ΔT is greater than 2°C, the adhesion of ice to the surface increases rapidly. The required low ΔT seriously decreases the heat transfer rate so that large heat transfer surfaces would be necessary in an operating system. In addition, the axial temperature gradient of the coolant in the freezer surface must necessarily be very low. These requirements would significantly constrain the evaporator design in a working system. If a refrigerant evaporator were used to make ice, it would have to be flooded, and its pressure precisely controlled. Alternatively, if a secondary fluid is used to make ice, then its flow rate would necessarily be large to minimize temperature gradients across the cool surface.

Another result of this research is that the density of ice formed by the self-release process is rather low. The ice formed by this technique is in the form of a fine slush. The density of ice crystals in a "filled" column of slush was found to be about 20% by volume, which is only about half the density obtainable with harvesting ice makers that are commercially available today.

2.2 Evaporative Heat Transfer

An experimental facility was built to measure boiling/evaporative heat transfer coefficients of a refrigerant flowing through a packed bed of energy storage media. This information is required to evaluate the suitability of phase change material as TES components on the refrigerant side of a heat pump. A search of the literature revealed no information available on evaporative heat transfer from a packed bed of spheres to a liquid-vapor working fluid.

An isometric of the facility is shown in Fig. 4. The test section is an aluminum cylinder 5 in. in diameter and 4 ft high. It contains numerous penetrations for instrumentation and visualization of the flow. Other major components are the pump, flow control valve, flow meters, pressurizer, water cooled condenser, and a 10-ft section of resistance heated pipe. Two glass spool pieces in the loop piping allow for visual monitoring of the flow. The working fluid is Refrigerant-113. Flow through the test section is downward. The bed was filled with random packed spheres. Two sphere diameters (5/8 and 1 in.) and two surface roughnesses were tested.

Heat transfer coefficients were measured using individual spheres that were equipped with an internal resistance heater and two surface thermocouples as shown in Fig. 5. Seven instrumented spheres of each size were fabricated and used in the tests. Initially, the spheres were polished with No. 400 emery paper (smooth surface). After completing these runs, the spheres were roughened with No. 40 emery paper and the tests repeated. The seven spheres were positioned in a nearly in-line arrangement and also in a cluster arrangement in the interior of the bed.

The sphere heat transfer coefficient measurement system was calibrated by operating the facility with water and R-113 in regimes where the heat transfer coefficient had been determined by others.[5] Specifically, the spheres were operated in the natural convection, forced convection (without boiling), and pool boiling regimes. In all cases, the measured heat transfer coefficient agreed quite well with the published coefficient. By way of example, Fig. 6 shows heat transfer coefficients as measured by the instrumented spheres under forced convection with R-113, compared to the published correlation by Baumeister and Bennett. Thus the heat transfer coefficient measurement system was determined to be adequate for the subject measurements.

The first series of tests was conducted at constant mass flow rate using smooth 5/8-in. spheres and R-113 under liquid-vapor flow conditions. For each mass flow rate, the inlet quality (mass fraction vapor) was adjusted to a desired value, and the influence of the surface superheat on the heat transfer coefficient was investigated. Here, surface superheat is defined as the temperature difference between the two-phase fluid and the surface of the heated,

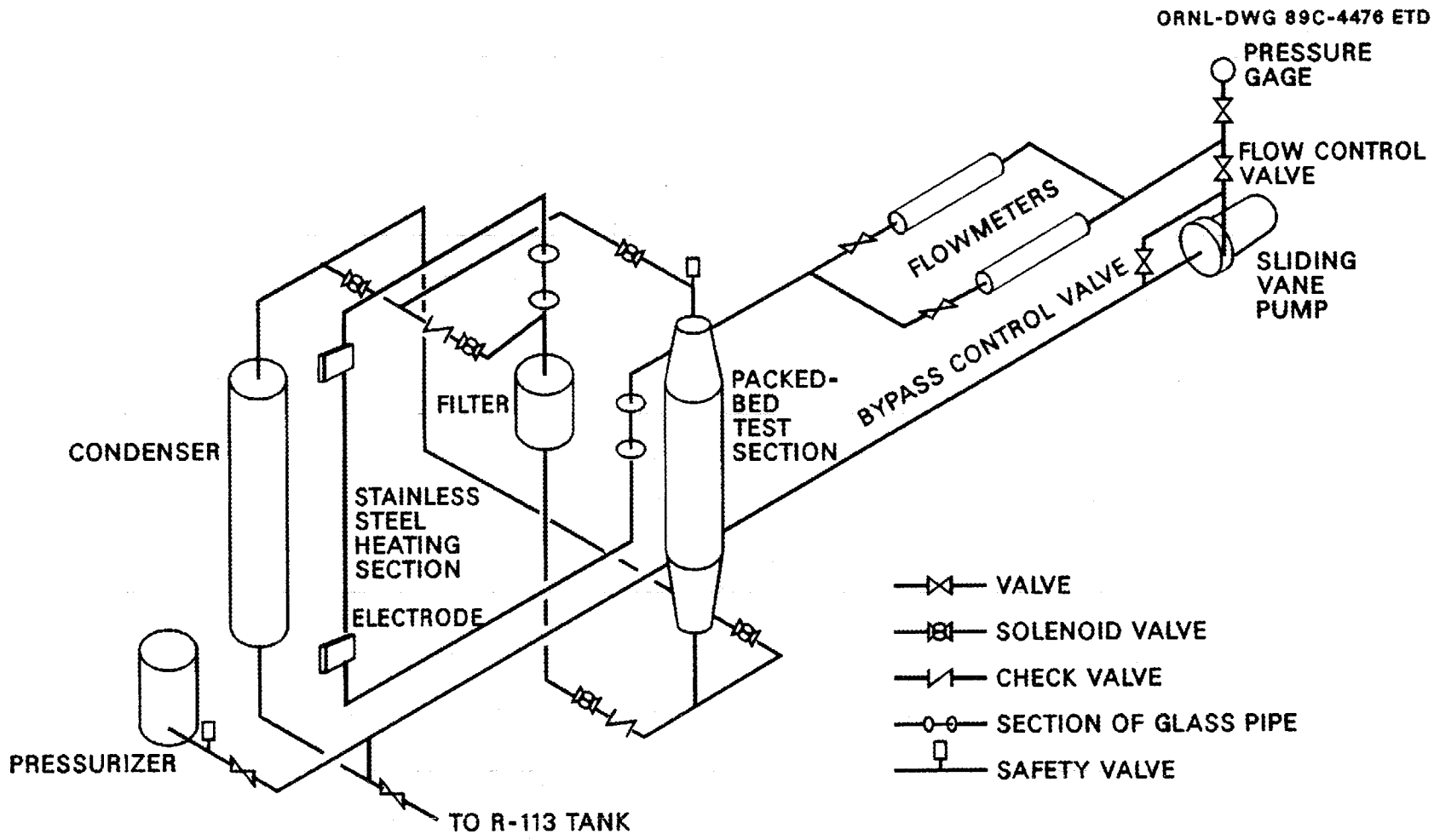

Fig. 4. Schematic layout of packed-bed evaporator test facility.

ORNL-DWG 90-3385 ETD

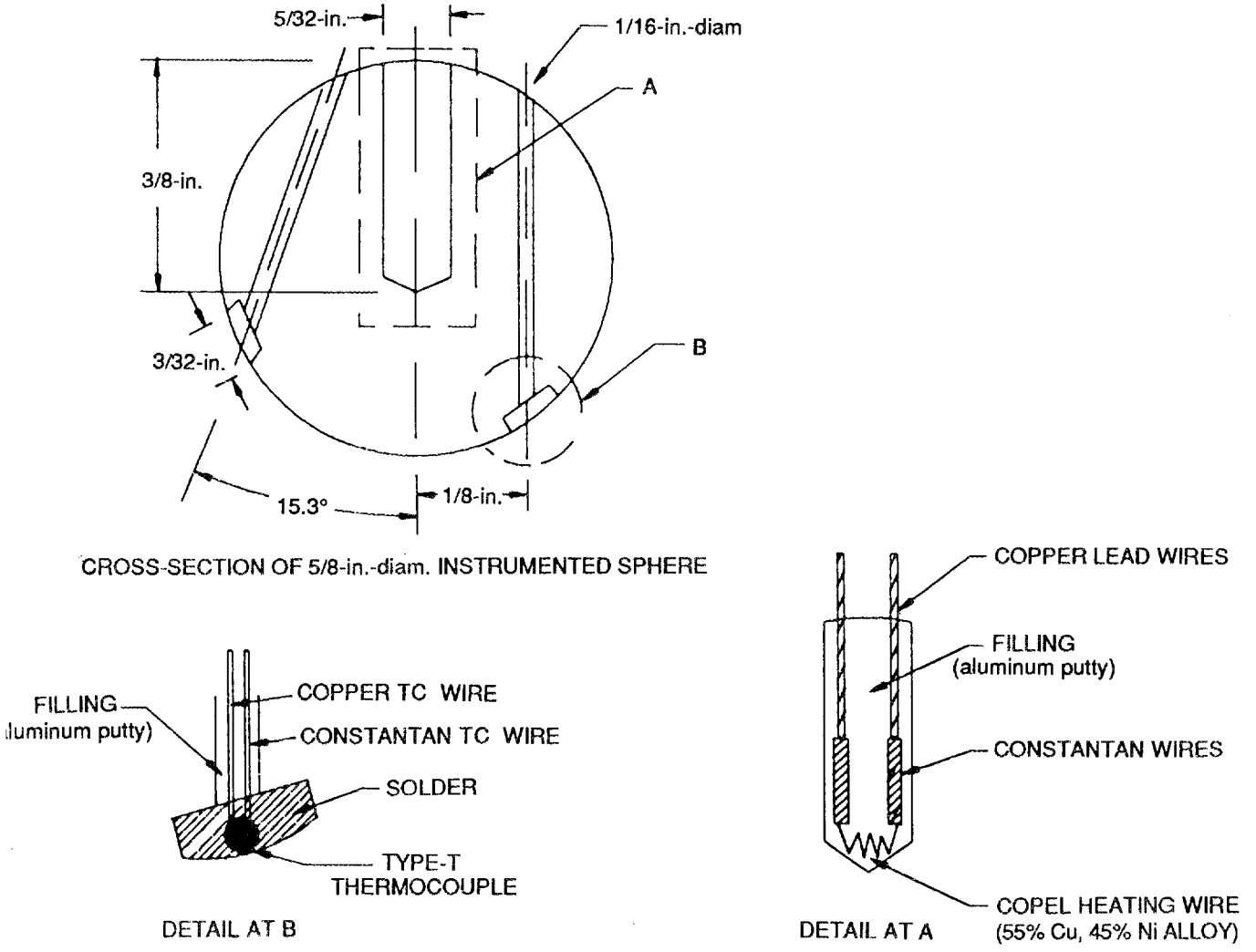

Fig. 5. Heat transfer probe and details.

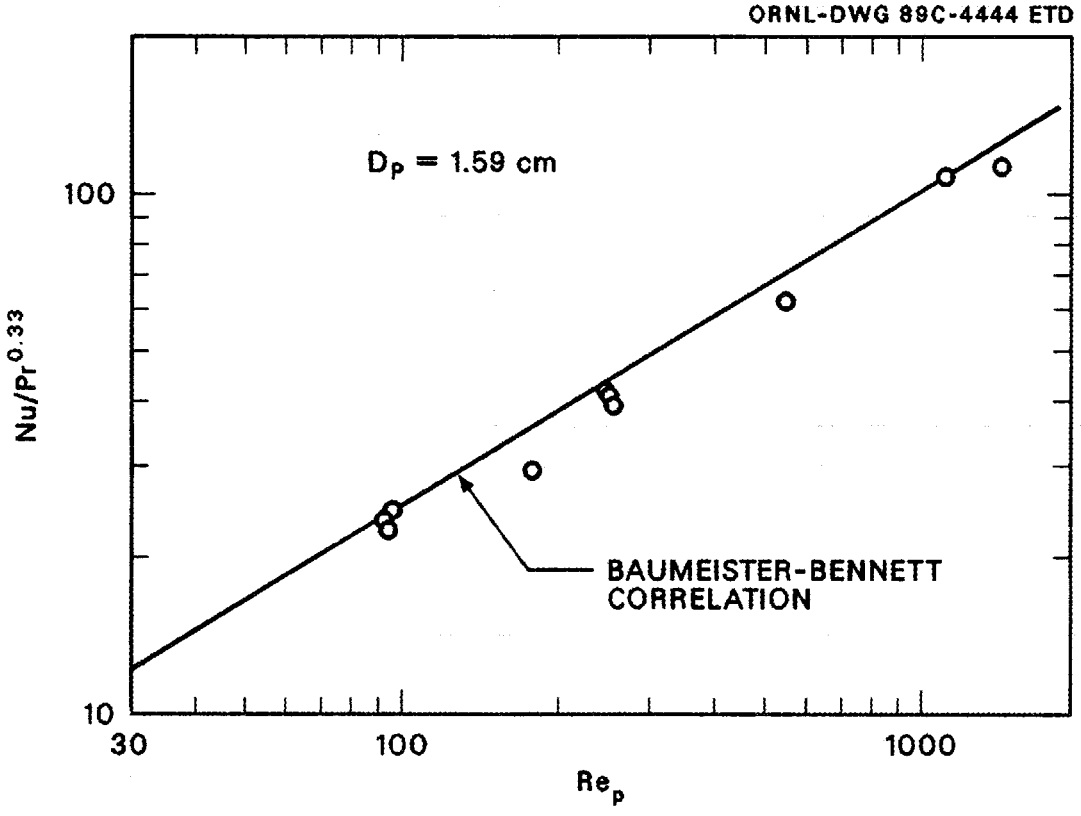

Fig. 6. Forced convection validation of heat transfer measurement system.

instrumented aluminum spheres. The heat transfer coefficient was determined at each inlet quality setting by changing the power input to the spheres and allowing the indicated temperatures to reach steady-state values. This procedure was followed for three inlet flow rates over a range of inlet qualities between zero and one. This series was than repeated for rough 5/8-in. spheres, smooth 1-in. spheres, and rough 1-in. spheres.

The ratio of the measured heat transfer coefficient under boiling conditions, h_{2P}, to the corresponding heat transfer coefficient for the homogeneous model, h_H, is correlated with the dimensionless surface superheat ΔT^*, the dimensionless heat flux to the instrumented spheres q^*, the liquid Reynolds number Re_L, and the inlet quality, x, to the packed bed. These quantities are all defined below. The heat transfer coefficient h_H for the homogeneous model is determined from the single-phase flow correlation of Baumeister and Bennett as given by:

$$\frac{h_H D_P}{k_H} = 1.58\ (Re_H)^{0.60}\ (Pr_H)^{0.33} \quad ,$$

where $$Re_H = \frac{\rho_H V_s D_P}{\mu_H}\ , \text{ and } Pr_H = \frac{c_{pH}\mu_H}{k_H} \quad .$$

The properties in the above equation are calculated using the homogeneous thermophysical properties of the flowing two-phase fluid as given by the following relations:

$$\rho_H = x\rho_v + (1 - x)\rho_L \ ,$$

$$\mu_H = x\mu_v + (1 - x)\mu_L \ ,$$

$$k_H = xk_v + (1 - x)k_L \ ,$$

$$c_{pH} = xc_{pv} + (1 - x)c_{pL} \ ,$$

$$V_s = \frac{m}{\rho_H A_t} \quad .$$

The properties are evaluated at saturation temperature of the fluid, and m is the actual (experimental) mass flow rate. It was hoped that the homogeneous model would take into account all of the influence of (1) quality via the use of homogeneous properties and (2) the mass flow rate and particle diameter via the Reynolds number Re_H. The results, however, indicate otherwise.

The correlation of the present results for the boiling heat transfer coefficients from spheres in packed beds is given below in dimensionless form:

$$\frac{h_{2P}}{h_H} = 0.2712\ (\Delta T^{*-1.132})\ (q^{*1.103})\ (Re_L^{-0.604})\ (x^{0.175}).$$

In physical variables, the correlation may also be written as:

$$\frac{h_{2P}}{h_H} = 0.2712 \left[\frac{(T_w - T_{sat})c_{pL}}{H_{Lv}}\right]^{-1.132} \left(\frac{qc_{pL}D_P}{k_L H_{Lv}}\right)^{1.103} \left(\frac{mD_P}{A_t \mu_L}\right)^{-0.604} (x^{0.175}) ,$$

where:

A_t	Cross-sectional area of bed $= \pi D_t^2/4$
c_p	Specific heat at constant pressure
D_P	Sphere diameter
D_t	Inside diameter of bed
h	Heat transfer coefficient
H	Specific enthalpy
H_{Lv}	Latent heat of vaporization
k	Thermal conductivity
m	Mass flow rate
q	Heat flux
q*	Dimensionless heat flux $= \frac{qD_P^2}{mH_{Lv}}$
Re	Reynolds Number based on particle diameter
V_s	Superficial velocity in packed bed $= m/A_t$
x	Quality (mass of vapor)/(total mass of liquid and vapor)
ΔT^*	Dimensionless temperature difference $= \frac{(T_w - T_{sat})c_{pL}}{H_{Lv}}$

<u>Greek Symbols</u>

ρ	Density
μ	Dynamic viscosity

Subscripts

2P	Two-phase (boiling) fluid
H	Homogeneous model
L	Saturated liquid
v	Saturated vapor
sat	Saturation conditions
w	Condition at the surface of the sphere.

Figures 7 and 8 show the fit of the above equations to the total data collected during these experiments.

2.3 Effect of Dopants on Solid State PCMs

The objective of this research project is to develop solid state phase change materials for thermal energy storage. Current research involves investigations of organic polyalcohol materials which undergo solid-solid phase transformation storing large amounts of (latent) heat per unit mass at a constant transition temperature which is well below their melting points. The known polyalcohols have high transition temperatures, and adjustment of the transition temperature is important to develop practical materials. This is possible by introducing substitutional and interstitial dopants to strain the lattice of the host material which results in lowering the transition temperature.

Polyalcohols are referred to as "plastic crystals" implying the plastically deformable behavior of the high temperature phase in which the energy is stored. There are four known important polyalcohols: pentaerythritol [PE] ($C_5H_{15}O_4$), pentaglycerine [PG] ($C_5H_{12}O_3$), neopentylglycol [NPG] ($C_5H_{12}O_2$), and neopentylalcohol ($C_5H_{12}O$). The first three are potential candidates and model materials for thermal energy storage. A few other related pure organic compounds, such as trimethylol propane [TMP] ($C_6H_{14}O_3$) and 2-amino 2-methyl 1,3 propanediol [AMPL] ($C_4H_{14}NO_2$), are of significance and are used as substitutional dopants. This research has only recently been initiated, and thus far, work has only been conducted on pentaglycerine.

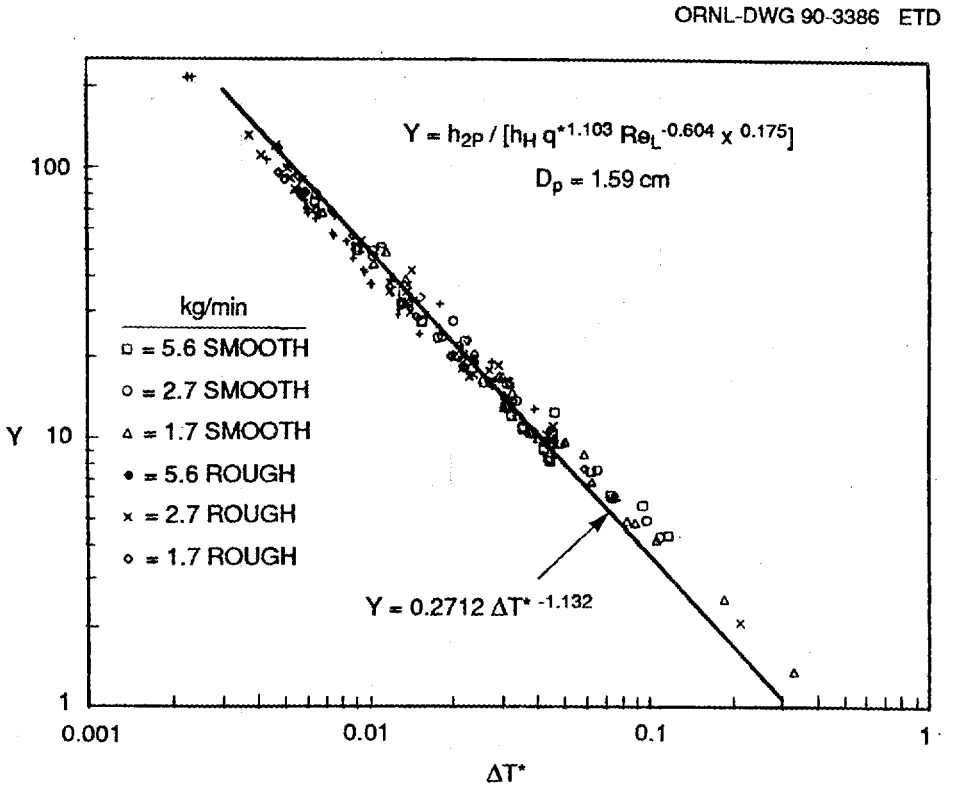

Fig. 7. Variation of boiling results with ΔT^* and comparison with present correlation; 1.59 cm spheres in cluster.

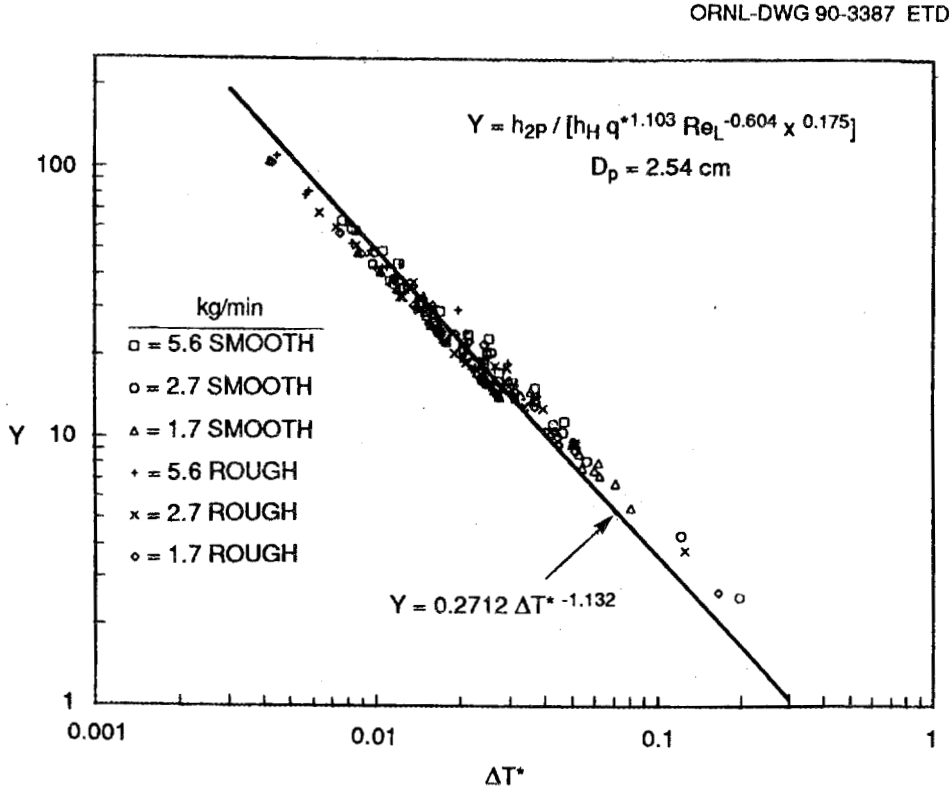

Fig. 8. Variation of boiling results with ΔT^* and comparison with present correlation; 2.54 cm spheres in cluster.

The properties of pure pentaglycerine are as follows:

Formula: CH_3-C-$(CH_2OH)_3$.

Solid Transition Temperature: 89°C (192°F).

Heat of Transition: 46 cal/g, 83 Btu/lb.

Crystal Structure: Tetragonal and Cubic.

Thermal analyses of the doped samples were first performed on a Perkin Elmer differential scanning calorimeter (DSC) using milligram-range sample sizes. The heating rate used was 10°C/min. Emphasis was on observing solid-solid transformation, and enthalpy versus temperature plots were obtained for these transitions. The sampling for the DSC work (4 to 10 mg) is very critical where two phases may be present in the doped samples. Often the amount of each phase is not representative and problems arise in interpretation of results. Therefore, a simple bulk technique was devised in which 6 to 10 g of doped material is placed in the glass test tube with a thermocouple placed in the center of the tube. Temperature vs time output was obtained on a chart recorder, and the plots were later digitized. In this system, sample errors are eliminated and a visual track can also be maintained to observe the phase changes, particularly for the solid-solid or solid-liquid type transformations. In fact, in most cases, one can distinguish between α and γ solid phases. It has been found that these results are reproducible and can be used to measure the transition temperature. The true transformation enthalpies are measured using the DSC, but rough estimations can be made by the bulk techniques also.

Several substitutional dopants were used to lower the transition temperature of PG. The TMP and AMPL dopants were effective in reducing the transformation temperatures, while dopants, such as glycerine, xylitol, and other stearates were not effective. Table 1 shows the results of these experiments. A solid solution series was made with PG/TMP and DSC, as well as the bulk thermal analyses methods were used to evaluate the phase transformation. The transition temperature observed from the bulk experiment and DSC are listed. In some cases, the discrepancies in transition temperature between the DSC and bulk sample data are attributed to the very small, milligram range sampling problems in the DSC analyses. The transition temperatures obtained from the bulk samples were reproducible. Note from Table 1

Table 1. Thermal data on doped pentaglycerine samples.

Materials	Solid-Solid Transition Temperature T_t(°C) Bulk	DSC	ΔH_t (cal/g)	Solid-Liquid Melting Temperature (°C)
5% TMP	-	84.02	40.58	-
10% TMP	83.5	83.63	37.72	184
20% TMP	80.5	83.92	38.11	167
30% TMP	73	84.17	40.62	152
40% TMP	70	81.78	37.65	138
50% TMP	65	78.36	31.65	120
60% TMP	52	52.01	31.52	103
70% TMP	43	-	35.00	83
80% TMP	25	-	-	68
5% AMPL	-	-	36.54	192
20% AMPL	61	76.10	-	192
30% AMPL	42	85.00	-	183
40% AMPL	18	-	-	177
50% AMPL	-	-	-	170
AMPL(PURE)	78	-	37.04	120
5% Xylitol	-	84.04	36.34	-
10% Xylitol	-	84.22	25.50	-
20% Xylitol	-	84.27	23.28	-
30% Xylitol	-	79.70	49.75	-
5% Glycerol	-	83.76	34.96	-
10% Glycerol	-	83.88	34.51	-
20% Glycerol	-	83.69	22.87	-
30% Glycerol	-	82.82	13.69	-
BRIJ52	-	84.66	32.10	-
BRIJ78	-	85.17	30.10	-
BRIJ102	-	85.10	31.68	-

that TMP and AMPL can effectively reduce the transition temperature of PG and still maintain a substantial heat of transition.

X-ray defraction techniques were used to evaluate changes in the crystal structure and also thermal expansion of the doped PG as a function at temperature. This data confirmed that the phase transformation of PG occurred, as expected, from the tetragonal (BCT) to cubic (FCC). Measured thermal expansion characteristics of undoped PG and PE are shown in Fig. 9. Thermal expansion in the α phase of PG is low, 0.51% at 78°C in the a-direction, while the expansion in the c-direction of the crystal was 0.04% at 78°C. This result was rather surprising, since one expects a rather large expansion in the c-direction because of the layering. The thermal expansion results of pentaerythritol, PE, whose crystal structure and layering is similar to that of PG was compared with results from previous work,[6] and it was found that the expansion in the c-direction was quite large in the α phase of PE as illustrated in Fig. 9. The reason for the low expansion coefficient in the c-direction of PG is unresolved, and there is concern that the structure in this phase is not truly BCT.

2.4 Liquid-Liquid Systems for TES

Several investigators[7] have suggested the use of liquid-liquid systems of limited miscibility to store thermal energy. As the fluid system cycles in temperature from a two-phase region to a single-phase region (near its critical solution temperature), the heat capacity of the fluid system is enhanced by the heat of solution. Thus the effective heat capacity of the fluid system is abnormally high. This concept is under investigation by the New York Polytechnic Institute. The initial phase of this effort consisted of identifying appropriate liquids for storage of heat and cold and measuring the heat of mixing for the most attractive systems. The theoretical basis of this concept has been described, and many of the measured heat of solution plots have been reported earlier.[8] Emphasis during this reporting period are on three-component systems. The purpose of the third component is to adjust the phase separation temperature to a more desirable value. Because of their low toxicity, mixtures containing glycol or glycol derivatives were primarily considered.

ORNL-DWG 90-3388 ETD

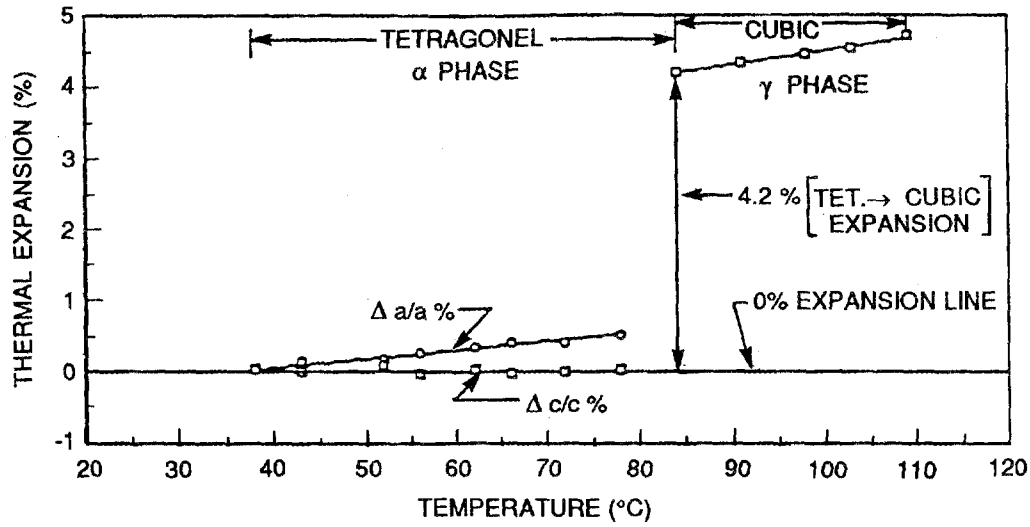

(a) THERMAL EXPANSION IN UNDOPED PG

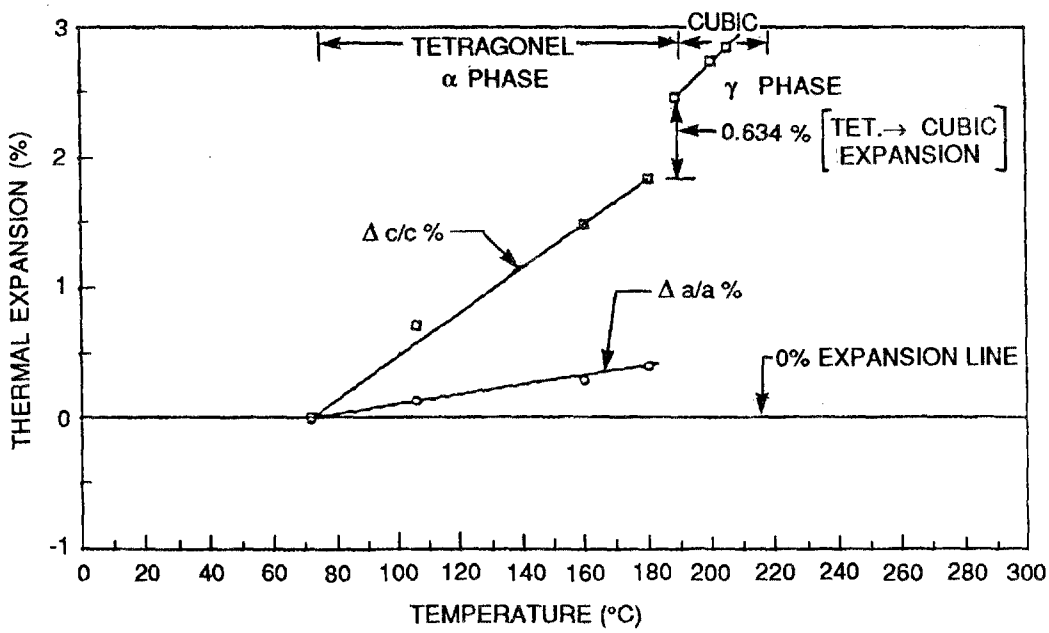

(b) THERMAL EXPANSION IN UNDOPED PE

Fig. 9. Thermal expansions in pentaglycerine (PG) and pentaerythritol (PE) in a- and c-directions.

Lower critical solution temperatures (LCST) of aqueous systems containing mixtures of glycols are determined principally by the phase behavior of the high molecular weight glycol constituent. Because the binary aqueous mixtures studied with lower molecular weight glycols have LCST values either higher or lower than the desired range (5 to 10°C), ternary systems with blends of glycols were used in order to obtain optimum temperatures.

Heats of mixing were found more difficult to obtain for multicomponent mixtures than for binary systems. In order to evaluate the contribution of the heat of mixing to the glycol blends, heat of mixing values were measured for the ethylene glycol diethyl ether-polypropylene glycol (mol. wt 725) system. The heats of mixing for this system were found to be small and exhibited no variation with temperature. Therefore, in this study the ternary mixtures were treated as effective binary systems, neglecting the small contributions to the heats of mixing for the glycol components. Heats of mixing measurements for ternary systems were conducted by mixing the two glycol components in the desired ratio and introducing the mixture into one of the flow calorimeter pumps. Distilled water was passed through the other flow calorimeter pump, and the measurements were initiated.

A list of the blends used in this study, the ratios of the glycol components by volume, and their molecular weights are shown in Table 2. Approximate values of the LCST for the ternary systems were obtained by phase equilibrium tests and are included in Table 2. The addition of diethylene glycol diethyl ether to ethylene glycol diethyl ether-water raised the LCST to about 2°C, but the ternary system did not exhibit as large a variation in the heat of mixing as the original binary system. In order to reduce the molecular weight of the polypropylene glycol (mol. wt 725) - water system, ternary mixtures were formed by adding, respectively, ethylene glycol diethyl ether, diethylene glycol diethyl ether, and polypropylene glycol (mol. wt 425). The resulting ternary mixtures did not exhibit as large an increase in the effective heat capacity between 5 and 10°C as did the higher molecular weight binary system.

Alternate three-component systems were also investigated. Through these and other tests with alternate three-component systems it was determined that the addition of a third component to a mixture can increase or decrease the phase separation temperatures. Third

Table 2. Aqueous systems with glycol mixtures.

Glycols Mixture	Ratio	Molecular Weight	LCST (°C)
Ethylene glycol diethyl ether- Diethylene glycol diethyl ether	1:6	154.51	2
Ethylene glycol diethyl ether- Polypropylene glycol (mol. wt 725)	1:5	417.71	<0
Polypropylene glycol (mol. wt 725)- Diethylene glycol diethyl ether	1:3	205.18	8
Polypropylene glycol (mol. wt 725)- Polypropylene glycol (mol. wt 425)	1:3	474.16	15

components which are soluble in both initial components increase the separation temperatures, while third components which are only soluble in one of the initial components decrease the separation temperatures.

Since the triethylamine-water system (LCST ~ 18°C) exhibits large increases in the effective heat capacity near the critical region, the effect of the addition of small amounts of dipropyl amine, sodium chloride, and urea to this system was investigated. It was found that the largest decreases in the phase separation temperatures were obtained by the addition of sodium chloride, but the shape of the resulting phase curve would not be similar to that of the triethylamine-water system. However, it was also found from these experiments that the addition of urea resulted in a phase curve with close to the optimum shape shown by triethylamine-water. Based on these analyses, heats of mixing were measured for the ternary triethylamine-urea water system. It was found through phase equilibrium experiments that optimum results were obtained for initial mole fractions of urea in water, x_u^i, in the range 0.077 to 0.1. The value of the LCST for this system is about 5°C. Experimental heats of mixing for the ternary system with $x_u^i = 0.077$ are shown in Fig. 10. It can be seen that the heats of mixing of this system decrease dramatically in the range 5 to 25°C, with the largest decrease occurring between 10 and 15°C. At a mole fraction of triethylamine $x_1 = 0.122$, the experimental heats of mixing show an increase of 602 J/mol (19.413 J/g) between 10 and 15°C. This increase corresponds to an effective heat capacity of 7.231 J/g·°C and represents an enhancement of about 70% over the heat capacity of water in this temperature range.

Additional heats of mixing were measured for this mixture with $x_u^i = 0.1$. The LCST for this system is about 3°C. The experimental heats of mixing are shown in Fig. 11. It can be seen that substantial changes occur in the range 5 to 12°C. For a mole fraction of triethylamine $x_T = 0.2$ in the three-component system, an increase in the heat capacity of about 50% over that of water is indicated for this temperature range.

For a system that does not show optimum phase behavior as a binary mixture, the addition of a third component could improve the temperature variations of the heats of mixing.

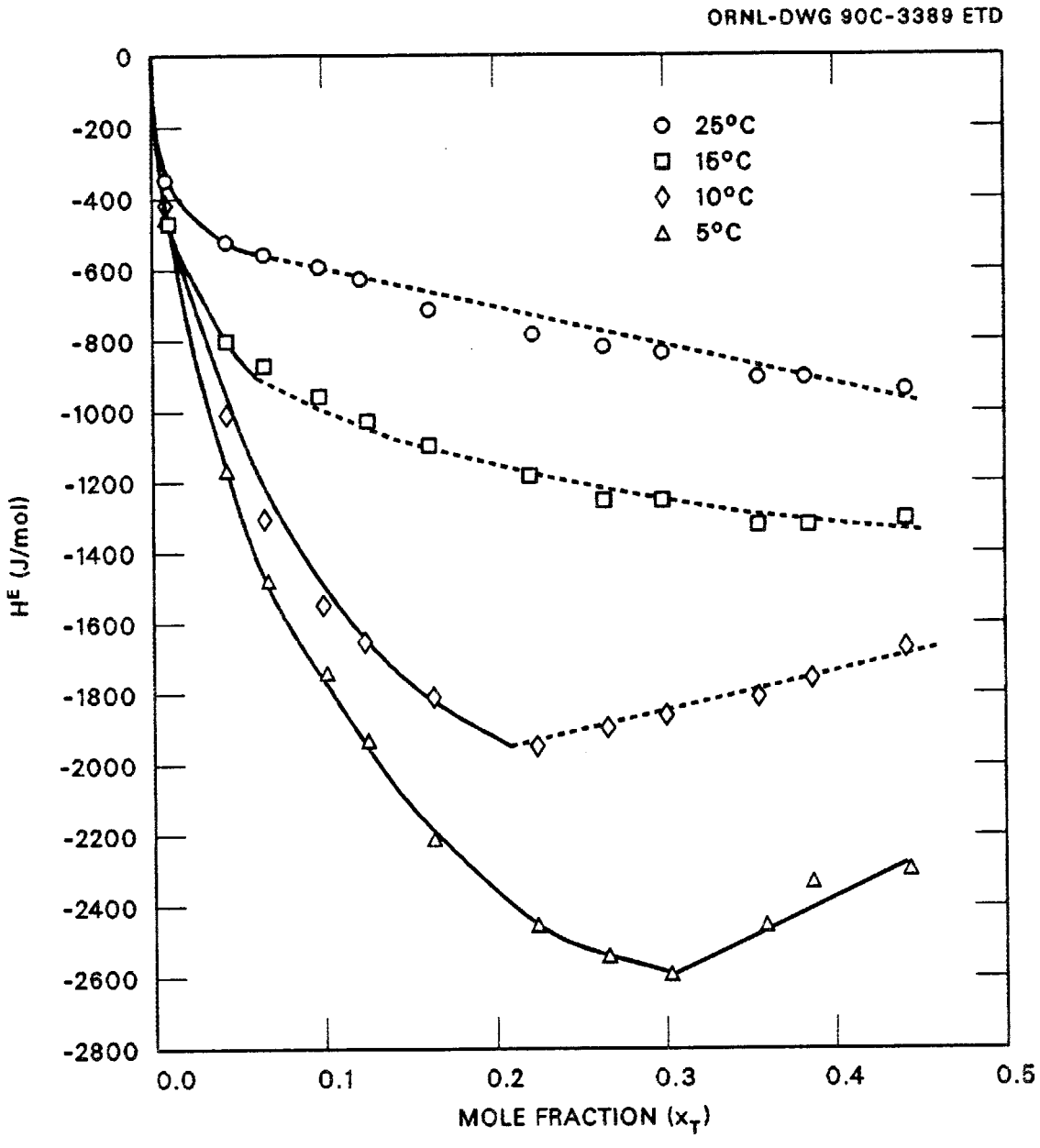

Fig. 10. Heats of mixing for triethylamine-urea-water; x'_u = 0.077.

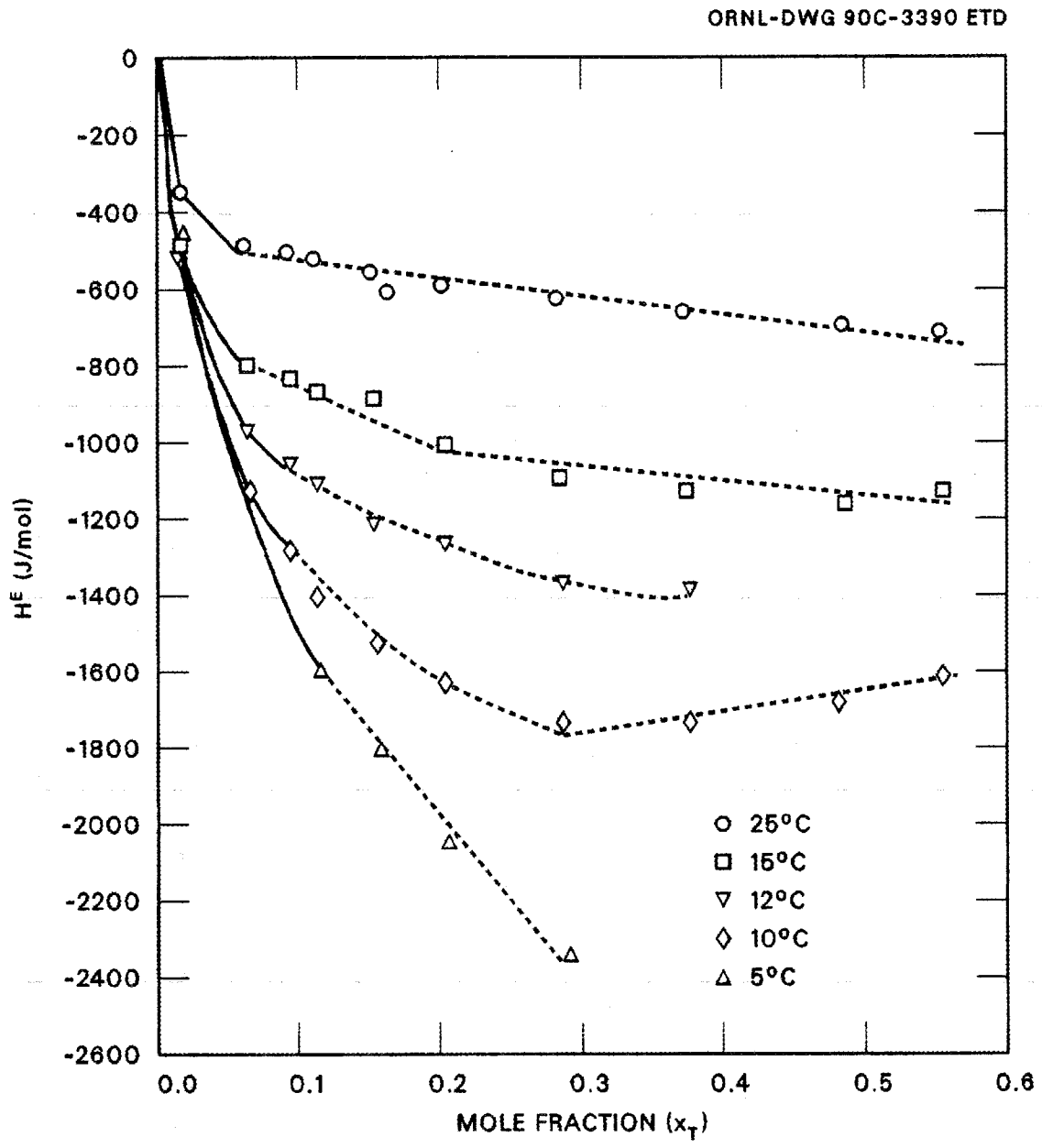

Fig. 11. Heats of mixing for triethylamine-urea-water; $x'_u = 0.1$.

In order to obtain a system with a suitable critical solution temperature and improved phase curve, the effect of the addition of sodium chloride to the diethylene glycol diethyl ether-water system was investigated. The critical solution temperature for the binary system was found to be about 25°C. The addition of sodium chloride to the binary system caused only small changes in the heats of mixing in the critical region. For an initial mole fraction ($x = 0.011$) of salt in water, the largest variations in the equilibrium phase compositions were found between 5 and 10°C. For this ternary system, the LCST is about 0°C.

Experimental heats of mixing for the three-component system diethylene glycol diethyl ether-NaCl-water are shown in Fig. 12 for 5 and 15°C. It can be seen that improved variations in the heat of mixing, compared to the binary mixture, occur for a glycol mole fraction of about 0.1. Although the effective heat capacity of the ternary system is slightly lower than that of water, it is improved compared to that of the binary diethylene glycol diethyl ether-water system for a comparable temperature range in the critical region. The important implication indicated by the results for this system is that the phase behavior of binary systems with LCSTs can be altered and improved for energy storage applications by the addition of small amounts of a salt or similar compound.

2.5 Computer Modeling of Building Materials Containing PCMs

It was noted in Section 1 that a principal thrust of the ORNL TES program is to improve the thermal performance of conventional building materials by using PCMs for increased energy storage. In support of this program, a computer model is being developed to analyze transient thermal transport and storage of both sensible and latent heat in multi-component materials. This program will be used to predict the performance of building materials containing PCMs for the passive solar and other applications and to determine favorable PCM parameter values for these applications.

Phase change and heat transfer processes in PCMs can be modeled in certain simple cases by known expressions for temperature distribution and phase change front location with time. For a broader class of processes, analytical approximations are available; however, these

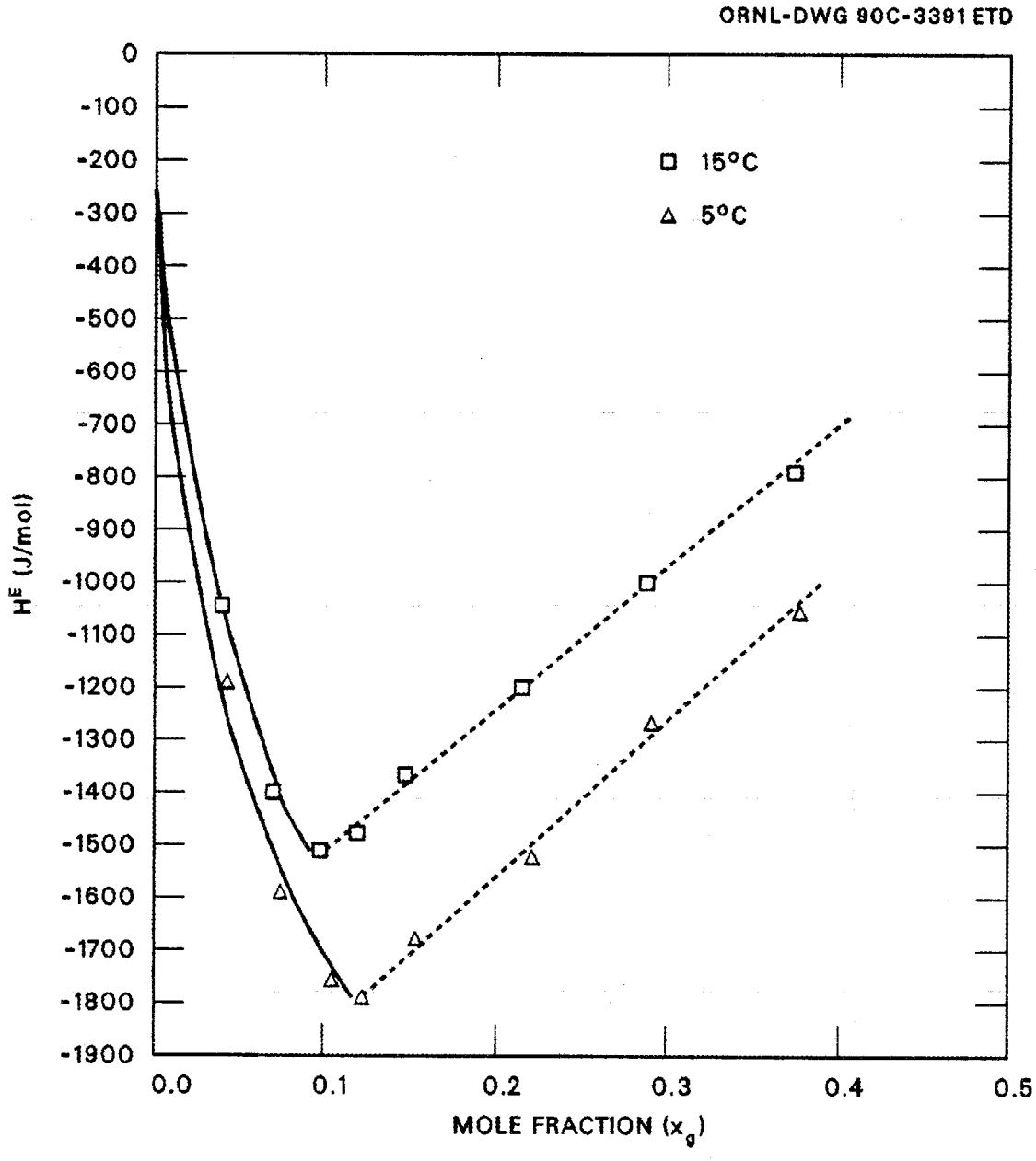

Fig. 12. Heats of mixing for diethylene glycol diethyl ether (1)-NaCl-water; x^i_{NaCl} = 0.0113.

methods must be used cautiously for they are capable of yielding physically unrealistic predictions of thermal behavior. Moreover, explicit solutions and analytical approximations are of limited help for the more general and combined boundary conditions as found in realistic thermal storage situations. Hence, numerical simulation is called for as the choice mathematical tool for analyzing the performance of a PCM-based thermal storage system.

The most effective means to simulate heat transfer and phase change processes in a PCM for general boundary conditions and arbitrary space dimensionality, is the so-called enthalpy method. This approach eliminates the need to pay explicit attention to the location of the front(s) separating liquid and solid regions and is based on local energy balances for control volumes into which the region of interest is subdivided. The thermal state of each control volume is "updated" through successive time steps enabling one to predict the evolution of the region beginning with some user-input initial state. Previous successful applications of this approach to storage situations include space station power system storage, passive thermal storage for a building structure, binary alloy solidification processes, solidification of super-cooled liquid, and pulsed laser annealing of silicon.

A computer program, WALL89, was prepared for the two-dimensional rectangular case of a wallboard. WALL89 can treat the PCM as if it were uniformly mixed with the matrix material or as if the PCM were present in the form of discrete pellets distributed throughout the solid support matrix. To each of the four faces of a region, WALL89 assigns time dependent boundary conditions of the form,

$$\text{flux in} = \text{convective flux} + \text{direct gain},$$

where convective flux is defined by a time-varying heat transfer coefficient and ambient temperature, and direct gain is defined by a time-varying flux function. An imposed face temperature is described by setting the heat transfer coefficient equal to infinity (its reciprocal equal to zero).

WALL89 is based on a subdivision of a rectangular region into small rectangular control volumes. The control volume size is set equal to or less than the "minimal lump size" of the PCM. The code begins by randomly distributing "lumps" among the control volumes in such a way that the final PCM volume fraction is equal to the desired user-input volume fraction value. This is done by an interaction procedure linked to a bisection method for volume fraction. The randomness of the method is based on the use of the computer random number generator, whose need is linked to the real time clock of the system, guaranteeing that for the same volume fraction, different PCM distributions will be generated for different runs. Each control volume consists either of PCM or matrix material.

Heat transfer and phase change processes are simulated by using the enthalpy (specific internal energy) as the key state variable to be updated. The enthalpy-temperature relations are different for matrix material and PCM. However, temperature is continuous with temperature gradients driving heat transfer. Thus internal energy is used to keep track of the thermal state of each control volume, while temperatures of control volumes drive internal energy changes. In updating the system state over a time interval, the boundary conditions drive heat into or out of the region, and conduction within the region alters the internal energy in each control volume. The enthalpy-temperature relation is then used to update the temperature in each control volume.

The numerical method used in WALL89 is a variant of an implicit numerical scheme due to Solomon et al.[9] The scheme is unconditionally stable for all time/space step combinations but for high levels of accuracy requires small control volume sizes. Actual runs of the code may take anywhere from minutes to hours depending on the desired accuracy and simulation duration. The code contains a rerun feature that allows the user to continue an earlier run from the point at which it ended, with its final state as the initial state for a subsequent run.

The BASIC language version of WALL89 includes graphics capabilities making it possible to visually track temperature profiles and PCM states with passing time during a program execution. The executable codes have been prepared for an IBM compatible computer.

2.6 Development of Complex-Compound Chill Storage System

The concept of a complex-compound chill TES system as described in an earlier progress report[8] operates on the chemisorption and desorption of ammonia by inorganic salts to form complex compounds. The process is accompanied by a substantial energy change. Emphasis during this reporting period was on development of the reactor heat exchangers.

Solid-gas chemisorption or adsorption reactions that are present in the chill TES concept are limited by heat and mass diffusion. Subcooling of the solid adsorbent leads to adsorption reactions, and superheating results in a corresponding desorption reaction. The degree of subcooling and superheating is an important determinate of the efficiency of a TES system. Therefore, heat and mass transfer resulting from thermal and mass diffusivities is an important process characteristic requiring significant attention in the development process. It is this heat and mass transfer limitation that has been the traditional problem in solid-vapor thermal processes and which has prevented commercialization of most thermal equipment development.

In the current study, three different approaches toward effective heat and mass transfer have been pursued in parallel: a slurry concept, a carrier liquid concept, and the dry bed reactor concept.

Slurry Concept

Since it was well known that heat and mass transfer rates of fixed bed reactions are largely dependent on bed thickness and resulting diffusion paths, the first attempt to improve heat and mass transfer properties was made by generating a slurry consisting of an ammonia-permeable liquid and an adsorbent salt that could be pumped across heat transfer surfaces. Several liquids were tested, and significant increases in reaction rates were observed. Figure 13 shows a reaction rate comparison between a conventional dry bed reactor and agitated slurry reactor. Further experimental tests revealed that pumpability of the candidate complex compounds can be maintained throughout the entire sorption process, if 35 wt. % liquid or

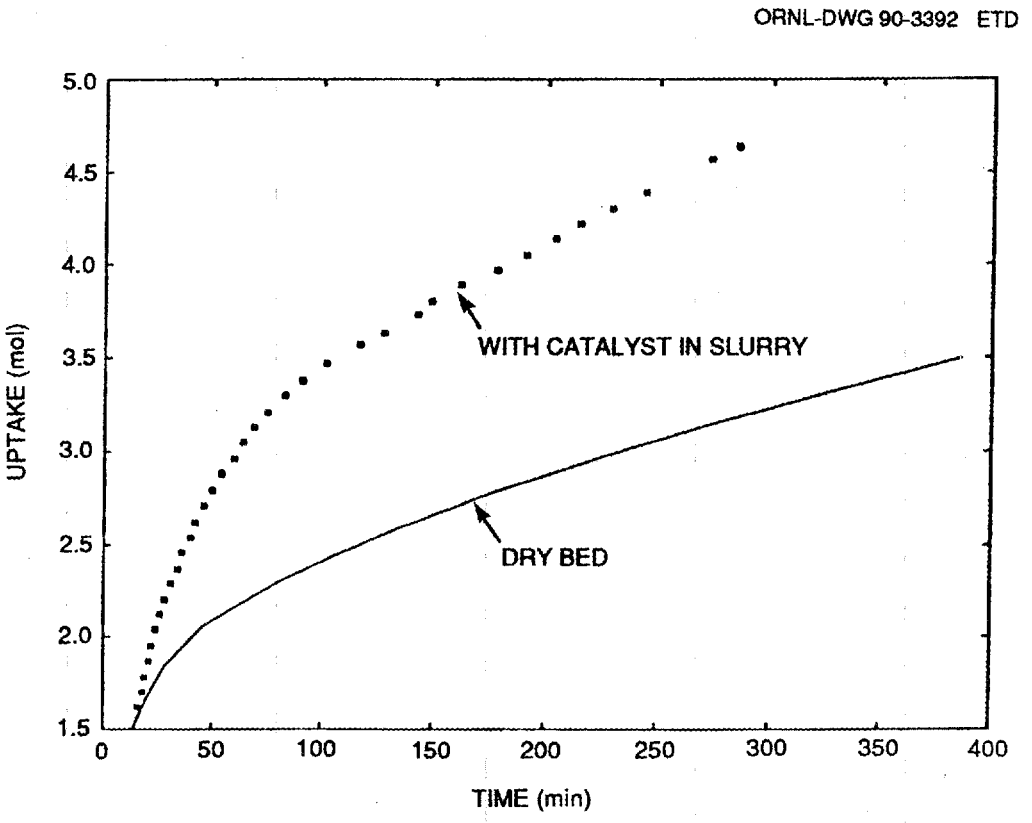

Fig. 13. Adsorption uptake curve for CC480

more of the carrier liquid is used with the adsorbent salts. This major reduction in heat transfer area due to the increased reactivities led to an improvement in the system economics. The technical problem to be solved centered around slurry conditioning and proper agitation. It was determined that slurry management was difficult and, because of success in the other approaches to heat and mass transfer, further exploration of this technique was discontinued.

Carrier Liquid Concept

Diffusivity can be enhanced by mechanically moving the solid adsorbent (as with the slurry concept) or by mechanically forcing a carrier liquid through a fixed bed of adsorbent, thereby enhancing heat transfer and ammonia transport. This approach was studied as a second technique for increasing the heat/mass transfer rates in the chemisorption system. Transport is effective if the carrier liquid has a high ammonia absorption capacity such that the ammonia refrigerant can be absorbed in a conventional liquid-vapor absorber and then released to the complex compound as the liquid is pushed through the solid bed. Since this technique was aimed at simplified fluid mechanics, a hardware loop was designed and operated to verify ease of liquid pumping through fixed beds of complex compound. While mechanical pumping and separation issues were settled, identification of suitable liquids proved difficult. In order for a liquid to qualify as a refrigerant carrier fluid, it must perform as an ammonia absorbent and therefore be soluble in ammonia; at the same time it should not dissolve a significant amount of absorbent salt, i.e., be inert to the absorbent. Several organics that fulfill the above criterion were identified. Sorption power of the carrier liquids for ammonia refrigerant, however, was limited such that reasonable ammonia uptake and transport could only be achieved at ammonia equilibrium temperatures of -1°C (30°F) or higher. Lower temperatures resulted either in low ammonia transport and excessive parasitic pump power requirements for the carrier liquid or, for liquids that showed high sorption capacity at low temperatures, the salt dissolved in the carrier liquid as it desorbed ammonia and was carried into the liquid vapor absorber. Since the technical approach using a liquid carrier fluid as the ammonia transport mechanism does not address the refrigeration target market with its typical operating temperatures at or below -7°C (20°F), investigation of this particular approach was discontinued.

Dry Bed Reactor

A third approach to optimize heat and mass transfer in solid-vapor complex compounds was investigated in parallel to the slurry-based approaches. This approach was based on a prior proprietary development in complex compound reactor hardware for industrial heat pumps. Solid-vapor reactivities having energy densities of 2 kW/kg and higher at approach temperatures (deviation from equilibrium) of only 8 to 11°C (14.5 to 20°F) were achieved. While these approach temperatures and reactivities were a significant breakthrough for solid-vapor heat pumps, applicability to boundary conditions suitable for thermal storage required verification. The duration of discharge and charge cycles of TES systems are typically several hours— one order of magnitude longer than found in heat pump cycles. This eases the reaction rate requirement accordingly by about one order of magnitude. However, the allowable approach temperatures for a cost effective thermal storage system are much lower than those tolerable in heat activated heat pumps. Therefore, the dry bed complex compound density control technique, which led to extremely promising heat pump reactor performances, was adapted to TES conditions with lower reaction rates and much lower approach temperatures. Two candidate complexes were investigated with respect to their desorption and adsorption reactions. Reaction rates of 0.7 mol/mol-h to 1.2 mol/mol-h constitute the desired range of reactivity. Figure 14 shows the results obtained with one of the candidate complex compounds. This complex can maintain a desorption rate of 1.5 mol/mol-h for a period of 220 minutes at approach temperatures of 4°C (7.2°F). This corresponds to a mole number change of 5.5, which is 75% of the theoretical coordination sphere capacity for this complex compound. Greater approach temperatures were found to permit higher rates or slightly larger mole number utilization.

Cycle Operation

Ammoniated, hydrated, alcohol, or ammonia complex compounds consisting of a solid metal salt and a gaseous refrigerant ligand are ideal reaction fluids for heat, cool, and chill storage systems. The multitude of salt adsorbents and refrigerant adsorbates make it possible

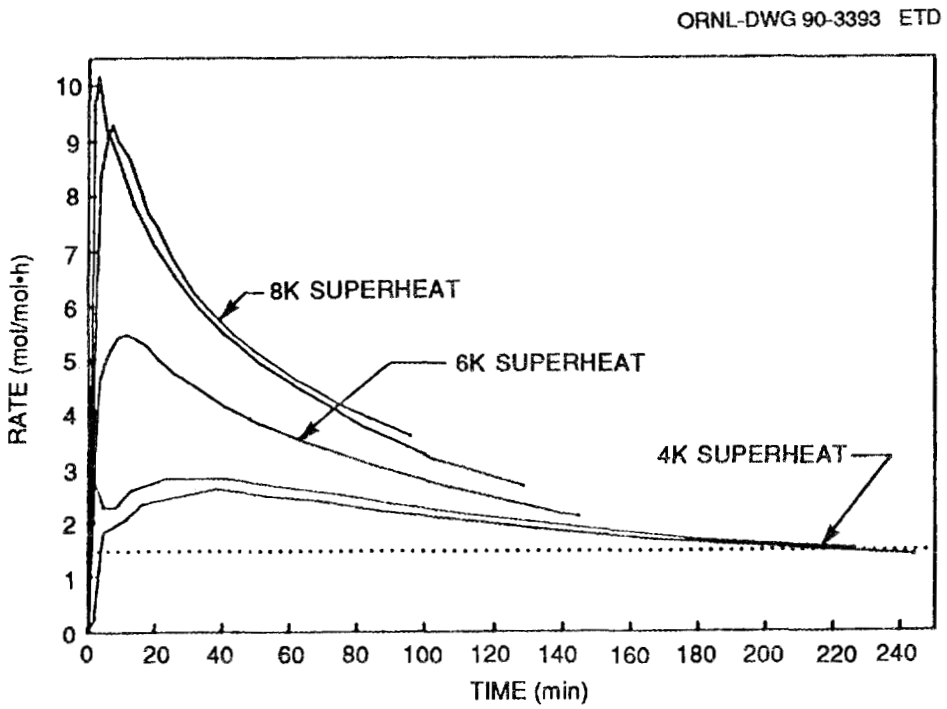

Fig. 14. Reactivity of CC180.

to cover a temperature range from approximately -60 to 600°F. Storage operation is possible by either pairing two single complex compounds or by using one complex and the plain ligand refrigerant. The systems can be designed as direct refrigerant contact or indirect thermally-coupled systems. The direct contact design uses the refrigerant of the vapor compression cycle as the ligand gas in the storage medium. This has the advantage of low heat transfer gradients but requires an almost oil-free refrigerant for the system. The indirect contact system is coupled to the refrigeration unit and/or a waste heat source across heat exchanger walls. This causes an additional temperature gradient, but it yields the safest integration of the storage system with existing chiller or refrigeration units.

Although chill storage systems can also be indirectly-coupled and heat actuated, most envisioned applications use a compressor to compress the ligand refrigerant which is in direct contact with the complex. The obvious refrigerant ligand for direct contact systems is ammonia, since it is commonly used as a refrigerant in compressor units as well as the ligand in complex compound formation.

Figure 15 shows the schematic of a compressor-actuated chill storage system. The system operates with one complex compound and the plain ligand refrigerant. Dual complex compound systems can be developed on the same basis. During discharge, the liquid ammonia ligand evaporates in the evaporator/condenser providing cooling through the associated heat exchanger. The vapor pressure of the ammonia at the low evaporator temperature, however, is still higher than the complex compound vapor pressure at the high heat rejection temperature maintained by an evaporative condenser or cooling tower. Therefore, the ammonia leaves the ligand storage tank, evaporates, and undergoes an exothermic adsorption reaction with the complex compound. Figure 16 shows the discharge process in the phase diagram.

In order to charge the system, the ammonia gas flow must be reversed. This can be obtained by either raising the ammonia pressure of the complex compound sufficiently high or cooling the condenser to condense the ammonia and ultimately lead the liquid back into the ligand storage tank. In any case, the pressure gradient must be reversed such that a positive

ORNL-DWG 90-3394 ETD

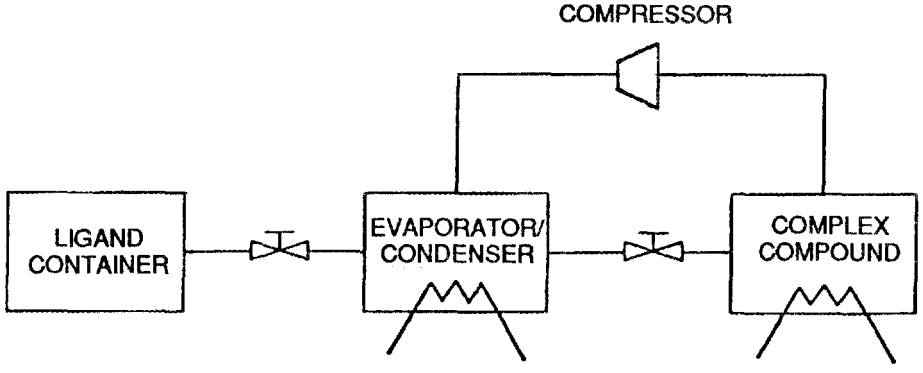

Fig. 15. Cool storage concept using compressor.

ORNL-DWG 90-3395 ETD

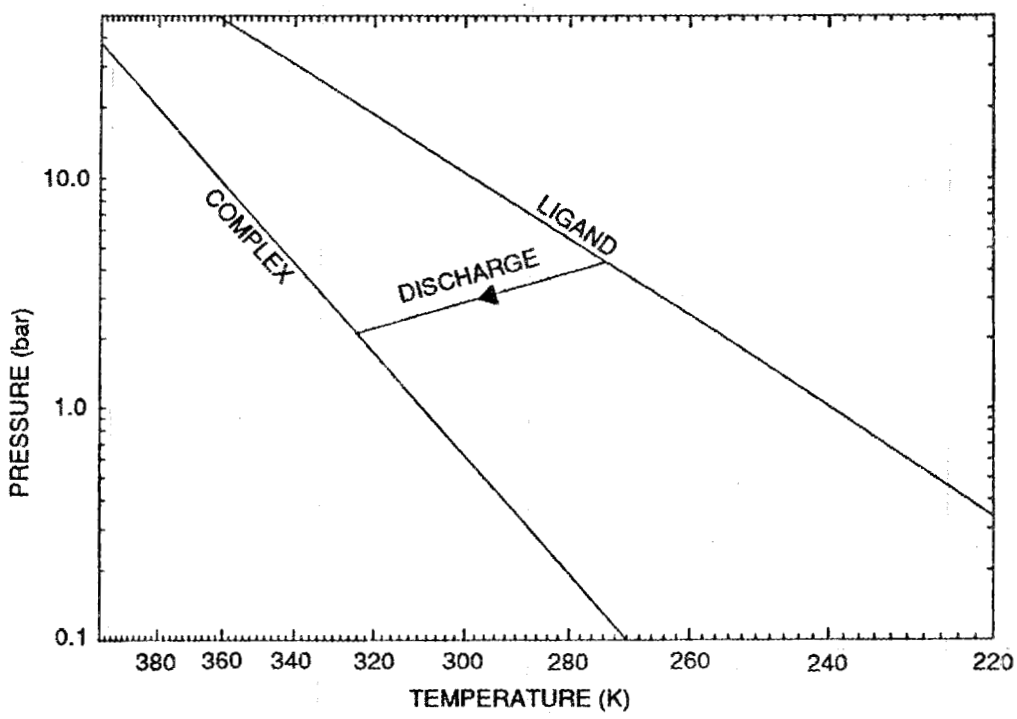

Fig. 16. Discharge of complex compound chill storage system.

ORNL-DWG 90-3396 ETD

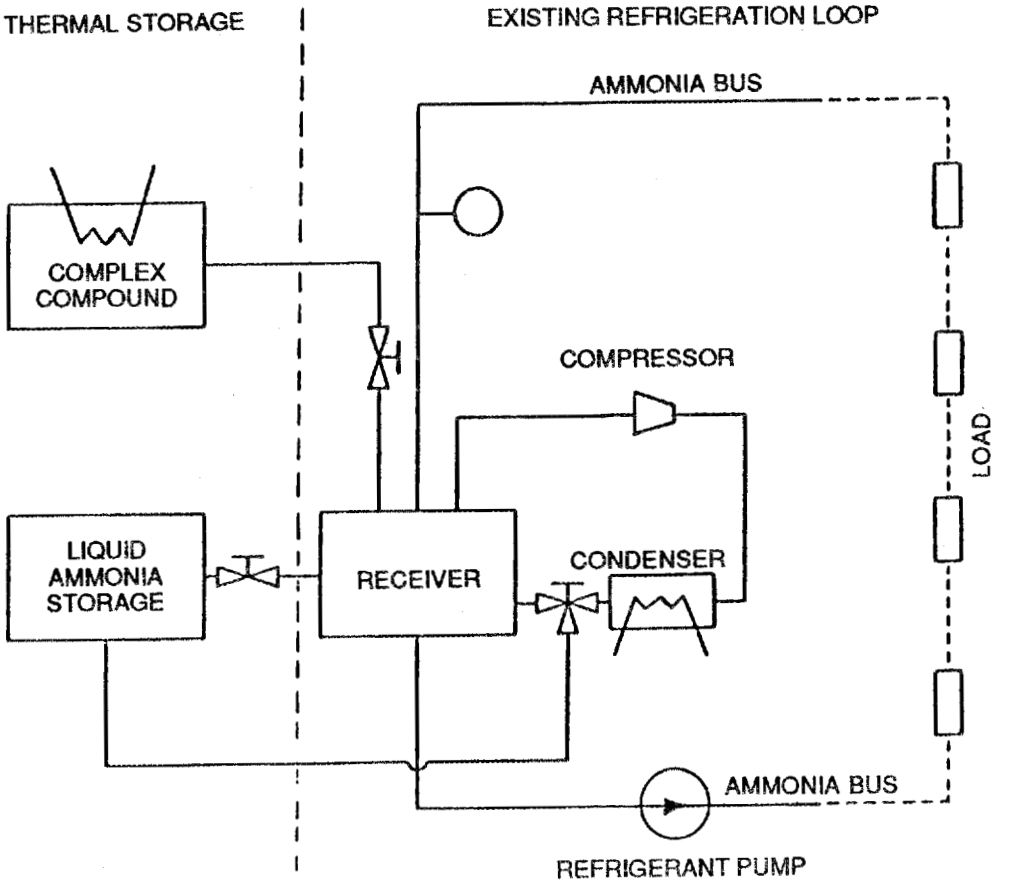

Fig. 17. Refrigeration loop with complex compound TES system.

flow of ammonia from the complex to the condenser can be maintained. If an existing vapor compression refrigeration system is used to charge the system, the ammonia is drawn out of the complex and fed into the low temperature receiver where it is picked up by the compressor. In order to maintain the design suction pressures, the complex must be heated with the chiller reject heat such that the low pressure receiver pressure is in approximate equilibrium with the complex compound ammonia pressure.

The most promising chill storage integration concept for an initial installation and field test is achieved by directly coupling with a low pressure receiver. Figure 17 shows a schematic of a directly-coupled TES system. During the charge process, the compressor is active, and ammonia gas leaves the complex compound reactor. Condenser heat is used to maintain the complex compound temperature around 35°C (95°F). During the discharge process, the compressor is not operating, and ammonia vapor is drawn from the receiver into the complex compound reactor. The complex compound temperature is maintained by means of the evaporative condenser or cooling tower.

Economics

Performance data on complex compound thermal storage systems are not available since the reactor systems are still under development. Cost predictions, however, were made based on the current development status. If no further performance improvement is obtained, cost for a -10 to -20°F thermal storage system, based on a 1000 ton-h capacity system, were estimated to be:

Adsorbent mass of CC180

24 kg/ton-h at $2.60/kg = $62.40/ton-h

Heat exchange surface

$3.50/kg adsorbent = $84.00/ton-h

Vessels and enclosures

$2.25/kg adsorbent = $54.00/ton-h.

The above costs are based on vendor quotes for technical grade salts, heat exchange surface, and ASME pressure vessels. This leads to a total of approximately $200/ton-h component cost. Installation and packaging costs were ascertained from manufacturers and application engineers. For a simple system integration, as envisioned for the thermal storage system, a mark up factor of 1.5 to 1.65 is to be expected. This leads to an estimated, installed cost of $300 to $330/ton-h.

The return on investment for the chill TES system is largely dependent on electric utility rates. The extremely low consumption of additional electric power during the charge process is one of the major advantages of complex compound thermal storage systems, which also simplifies the economic trade-off calculations. In utility areas with aggressive cool TES incentive programs, returns on investment exceeding 50% can be achieved. Where no purchase incentives exist, returns are lower but typically not below 30%. An extensive economic analysis has shown[10] that conventional cool TES systems with much higher electrical parasitic penalties save about $100/year and ton-h in utility expenses. Utility-sponsored chill TES incentives are typically restricted to $100,000. From these figures, a simplified economic analysis leads to a 30% return on investment in areas with no buying incentives and 45 to 50% in areas with active utility incentive programs.

2.7 Direct Contact Ice Storage System Development

The apparent advantages of direct contact heat exchange in ice making are twofold: (1) an improved operating efficiency due to very low approach temperatures and no defrosting requirement and (2) the potential for lower first cost through a reduction in the need for surface evaporators. Based on these advantages, the TES Program has continued the development of a direct contact system in which evaporating refrigerant impinges against a stream of water which freezes into ice. The obvious problem of moisture carryover into the refrigerant system

ORNL-DWG 90-3397 ETD

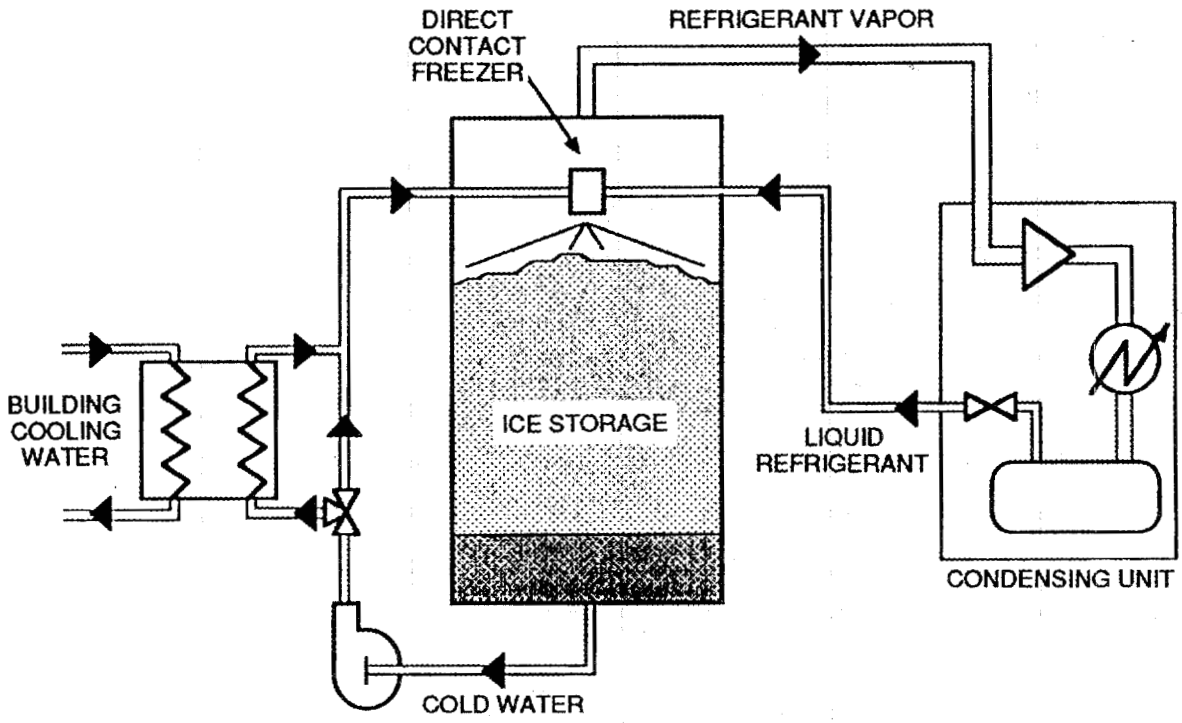

Fig. 18. Direct contact system flow schematic.

is being addressed by CBI Industries through the use of a compressor that can accommodate refrigerants saturated with water vapor. In this way, moisture carryover is tolerated rather than eliminated through the use of expensive separation systems. The key to this direct contact system is a liquid ring compressor that uses water as a sealant and coolant. R-114 was selected for the refrigerant based on its thermodynamic properties and the fact that it does not form a clathrate. During the reporting period, CBI successfully operated a 2½-ton prototype model of the system.

The next step to advance the understanding and technical development of the system is to build a full-sized model suitable for use in a commercial building. Thus CBI was funded to design, build, and test an advanced direct contact open refrigeration cycle ice production and storage system rated for 25 tons with approximately 300 ton-h of storage. A schematic of the system is shown in Fig. 18. Cold water is pumped from the bottom of the storage tank and into the direct contact freezer. Similarly, refrigerant from the condenser is sprayed into the direct contact freezer, where the two streams impact and ice is formed. The 25-ton unit will be tested in the laboratory for ice generation and storage characteristics, discharge characteristics, component performance, and materials compatibility. Modifications will be made, as necessary, to achieve the desired performance and reliability goals. Following these tests, it is planned to install the unit in a building for a long term reliability and performance study. At this time, the system design has been completed.

2.8 Incorporation of PCMs into Building Construction Materials

A major thrust of the ORNL-TES program involves the incorporation of PCMs into conventional building materials for the purpose of enhancing their energy storage capacity. The building material of current interest is gypsum wallboard. Such a material used in wood frame construction would increase the thermal mass in an otherwise low-mass structure. Although the principal application is passive solar, increased thermal mass in a habitable structure may be useful for a variety of reasons such as increased comfort and electrical load management.

Octadecane paraffin ($C_{18}H_{38}$) has been identified by the University of Dayton Research Institute (UDRI) as a promising PCM for the passive solar application.[11] Its melting point is about 23°C (73.4°F) which is slightly above room temperature. Moreover, the melting point can be tailored by mixing with other homologues of the same series. It has a substantial heat of fusion (~80 Btu/lb), and its melting and freezing characteristics are well behaved. In general, it is chemically, physically, and biologically inert and can be purchased for $0.25/lb to $0.50/lb in large quantities.

Octadecane wax in combination with building materials has been under development by UDRI for several years. They have developed two principal methods of adding the wax to plasterboard:

1. Fabricated wallboard is simply immersed in molten wax, and the wallboard absorbs wax like a sponge. Concentrations of wax as high as 35 wt % of the composite have been obtained by this method.

2. Wax can first be absorbed by crosslinked high-density polyethylene pellets which are then added to the mix used to manufacture wallboard. Wax concentrations in the composite are about the same as in the first method.

The advantage of the first method is that wax can be impregnated directly into the wallboard by anyone, whereas, in the second method the wax must be incorporated during wallboard manufacture. Although both methods have potential commercial interest, the first method is more convenient for development work.

A number of 4 x 8-ft sheets of wallboard were immersed in molten octadecane wax by ORNL and sent to UDRI for thermal stability testing. Figure 19 shows results of a Differential Scanning Calorimeter (DSC) run for the wax used in these tests. Note that the wax shows a single melting peak of 25.84°C and a double freezing peak at lower temperatures. The difference between the melting and freezing temperature probably results from thermal lag in

ORNL-DWG 90-3398 ETD

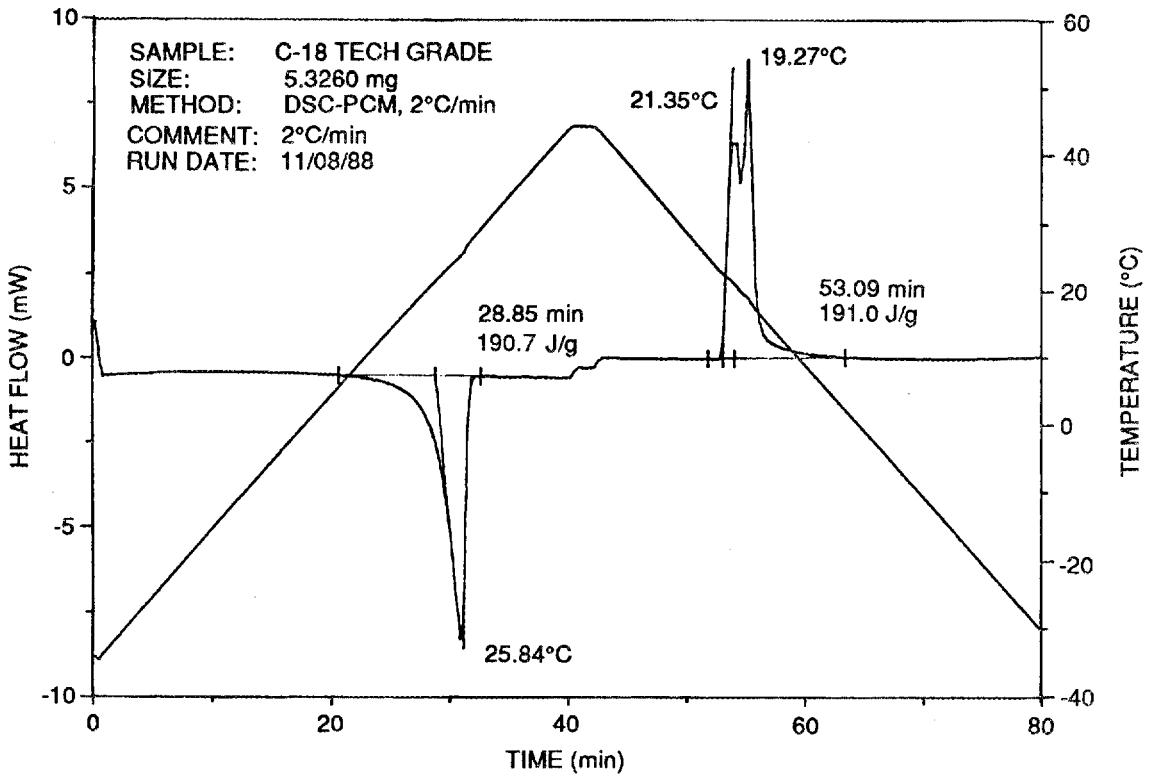

Fig. 19. DSC plot for n-Octadecane.

the DSC. Note also that the material melts and freezes over a range of temperatures which may be caused by the wax being 92% pure octadecane and containing about 4% each of $C_{16}H_{34}$ and $C_{20}H_{42}$.

There were two thermal stability tests conducted by UDRI. The first test consisted of maintaining the wax impregnated wallboards at an elevated temperature (100°F) with circulating hot air for an extended period of time. The second test consisted of thermal cycling the wax impregnated wallboards many times. Two kinds of cycles were conducted: Cycle A alternately cycles hot and cold air on opposite sides of the panels, and cycle B alternately cycles hot and cold air on the same side of the panels. In all tests, full-sized panels (4 x 8 ft) were used.

The wallboard samples were weighed before, during, and after the elevated temperature tests. In addition, DSC runs were made on sample drillings taken from the wallboard before and after the tests. Results of these tests are as follows:

1. There was no significant migration of the wax within the wallboard during this test.

2. During the course of this test, a small weight loss did occur as shown in Table 3. Part of the weight loss could be attributed to evaporation of moisture; however, some resulted from a slow evaporation of wax. This latter observation was confirmed by an oily condensate deposit that appeared on the cooler hinges of the containment box door. This is not considered a serious drawback for the intended application because the wallboard will normally be cooler, and the exposed surface will be painted or covered in some way.

3. The DSC results showed no change in the heat of fusion but did show a slight rise in melting point. This may be attributable to evaporation of the lighter wax component ($C_{16}H_{34}$).

Table 3. Weight loss of 1/2-in. wallboard aged 1, 2, and 3 months in air at 100°F

Board No.	% PCM by weight	Initial weight (lb)	Weight change (lb)		
			Month 1	Month 2	Month 3
B1	29.8	83.0	-1/8	-1/8	-1/4
B2	30.0	81 13/16	-3/16	-1/8	-1/4
B8	19.6	71 7/16	-3/16	no change	-1/4
B9	20.2	71 3/4	-1/4	-1/4	-1/4
B12	15.0	67 1/4	-1/4	no change	-1/4
B13	14.7	68 1/4	-3/8	-1/8	-1/4
Control (½ in.)	0	58 1/4	-1/8	no change	no change

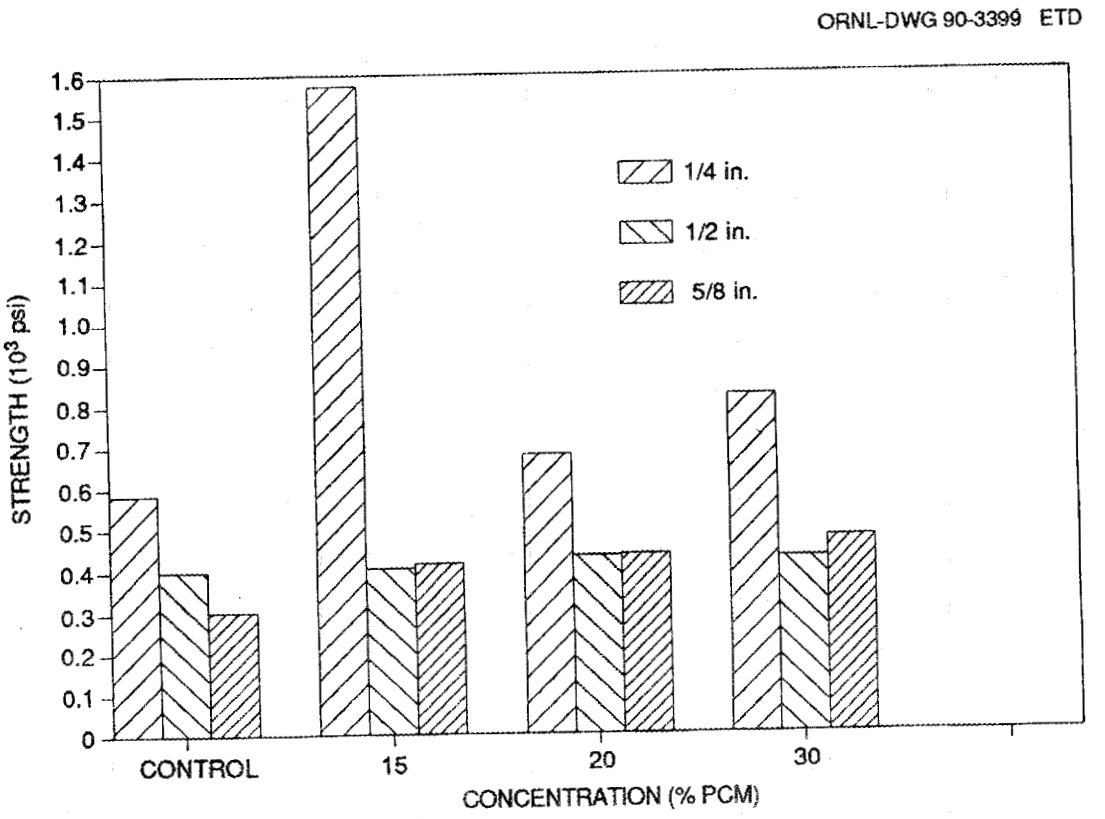

Fig. 20. Variation of flexural strength with concentration for three thicknesses.

Analysis of the wallboard for the cycling tests was conducted in a similar fashion as the elevated temperature tests; that is, by change of sample weight and by DSC analysis. Results of these tests are as follows:

1. There was no significant migration of wax within the wallboard during the tests.

2. There was no weight change of the samples during this test.

3. A "frost" sometimes appeared on the sample surfaces during the cool part of the cycle. The frost appeared to be similar to hoarfrost that one sees on cold winter mornings. The mass of wax involved was extremely small, and it could be eliminated by painting the surface or chemically cleaning the surface.

The flexural strength of wallboard with and without wax was measured and is described in Fig. 20. This plot shows the strength as a function of wax concentration in the wallboard and the thickness of the wallboard. In all cases, the flexural strength remained the same or increased with the addition of wax.

A number of small-scale screening tests were carried out concerning the flammability of wax impregnated wallboard and the effect of fire retardants. The results were sufficiently encouraging that a more meaningful series of tests, including a number of Steiner Tunnel tests, are now planned.

2.9 PCM Wallboard Fabrication and Testing

In support of the effort to develop conventional building materials that contain PCMs for increased energy storage, two technical tasks were conducted at ORNL:

ORNL-Photo 319-90 ETD

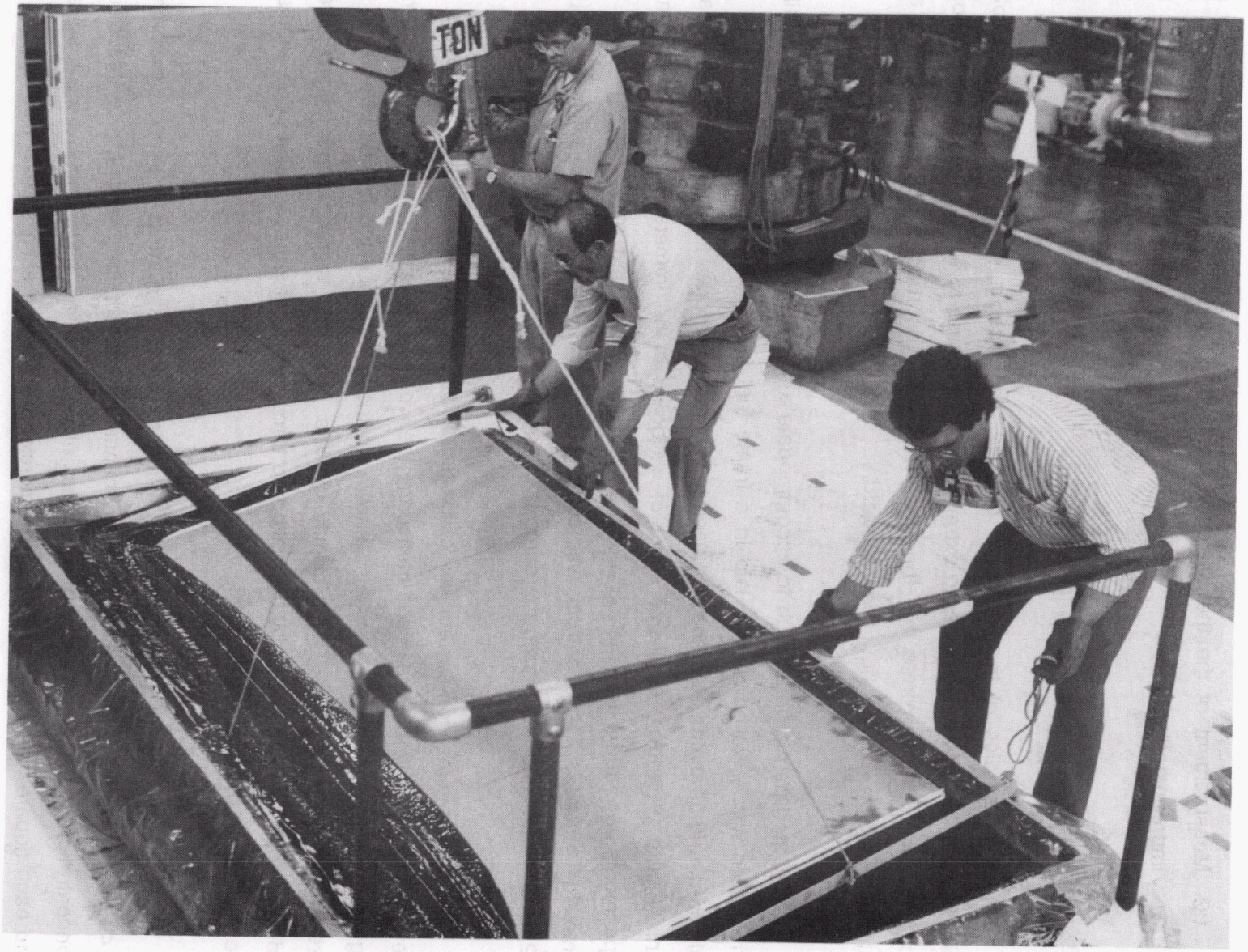

Fig. 21. Immersing wallboard in wax.

1. Scale-up of the immersion process to full-sized (4 x 8 ft) sheets of wallboard.

2. Measurement of the thermal conductivity and heat capacity of wallboard impregnated with wax.

Scale-Up of Immersion Process

All prior studies of the wallboard concept were accomplished with small samples, typically 1 x 1 ft. It was necessary to extrapolate this process to full-size sheets of wallboard (4 x 8 ft) and to demonstrate that the amount of wax absorbed could be controlled and distributed uniformly throughout the wallboard.

A heated pan large enough to accommodate a 4 x 8-ft sheet was fabricated and filled with molten wax. Wallboard was laid in a frame that featured a wire support bed for the wallboard, and an overhead crane was used to lower and withdraw the sheets from the heated pan. Figure 21 shows a full-size sheet of wallboard being immersed in the wax. In all experiments reported here, the octadecane wax was maintained at 170 to 175°F for the immersion process. The sheetrock was supplied by U.S. Gypsum in three thicknesses (1/4, 1/2, and 5/8 in.) and came from the same factory run.

The wax immersion system was calibrated by dipping 1 x 1-ft squares of wallboard into the wax bath for different times and measuring the weight increase. These data are shown in Fig. 22 for all three thicknesses. Also shown on these plots are the results of soaking full-size sheets of wallboard. The proximity of data points for samples and full-size sheets indicates the wax is absorbed by the wallboard through the flat surfaces, and edge effects on the absorption process are minimal.

The uniformity of wax distribution was also demonstrated in a second experiment. A 4 x 4-ft sheet of ½-in. wallboard was immersed in wax long enough to result in a concentration of 25.7 wt % wax in the product. The sheet was then cut into 1 x 1-ft squares, and each square was weighed. Before immersion in the wax, each square would have

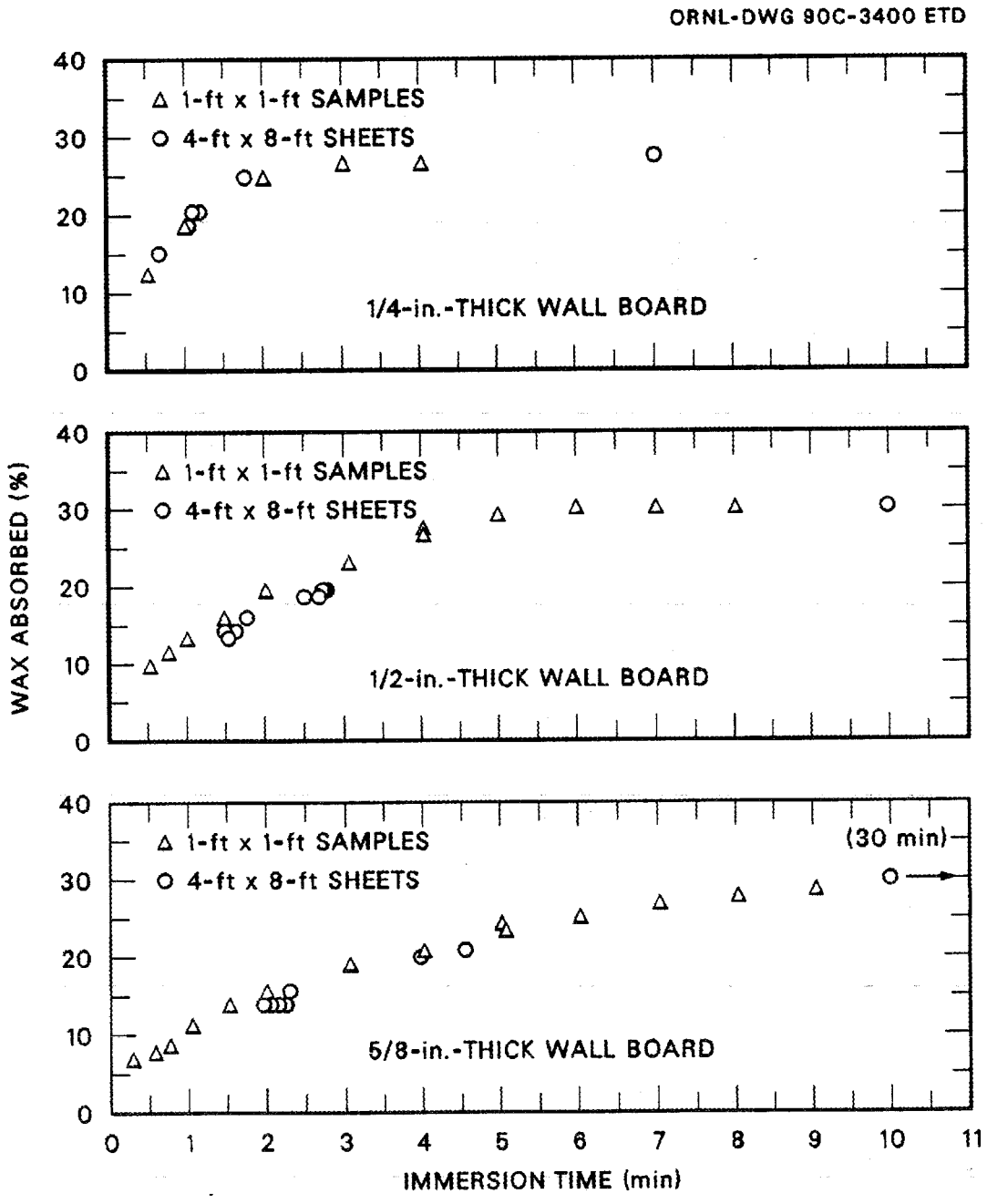

Fig. 22. Wax absorbed by wallboard as function of immersion time.

weighed approximately 810 g. After immersion, the average weight of the squares was 1090 g with a standard deviation of only 12.1 g. The conclusion was that the wax absorption was quite uniform over the flat surfaces of the wallboard.

Red dye (Oil Red O) was added to the wax so that after immersion, the wallboard could be broken and the penetration of the wax could be observed. Immediately after sample immersion, the wax was observed to be concentrated near the surfaces. However, if the wallboard was maintained at a temperature above the wax melting point for a period of time, the wax diffused, and the concentration became uniform across the thickness.

After demonstrating that the amount of wax absorbed could be controlled by the time of immersion in wax and that the wax was distributed uniformly throughout the wallboard, approximately 50 full-sized sheets were impregnated to achieve three concentrations (15%, 20%, and saturated). About half the wallboards were sent to the UDRI for thermal tests, and about half were retained by ORNL for internal development activities. Before the wallboards were used for any purposes, they were maintained at a temperature of at least 125°F for a period of time (one or more days) to allow the concentration across the thickness to become uniform.

Conductivity measurement and analytical model confirmation

As previously described, an analytical model was developed to study heat transfer and storage in wallboard containing a PCM. In order to have confidence in this model, it was necessary to know accurately the thermal conductivity of wax impregnated wallboard above and below melting point and experimentally to validate the model.

An existing ORNL facility which was designed specifically to measure the thermal conductivity of building insulating materials was used to conduct these experiments. The facility shown in Fig. 23 consists of a centrally located screen wire resistance heater with building material samples on both sides (two-directional heat flow) and cooled copper plates on the outside of both samples. The screen wire heater has dimensions of 3 x 5 ft, and the

2 x 3-ft samples were framed with insulation. Thus near the center of the assembly, heat flow was axial so that edge effects could be neglected. The facility was built such that the minimum sample thickness that can be tested is approximately 1½ in. Therefore, for the ½-in. wallboard tests, a stack of four sheets was required above and below the resistance heater.

The thermal conductivity of wallboard containing 0, 15, and 30% wax was measured, and the results, shown in Fig. 24, indicate that the conductivity of wax impregnated boards is slightly higher when the wax is frozen than when the wax is molten.

A series of transient tests to confirm the analytical model were planned. The first test will be one in which the samples are allowed to equilibrate to the temperature of the cool plates. At time zero, the screen heater will experience a step change in temperature imposing a temperature gradient across each sample. The temperature at locations on the surfaces and interior of the samples will be measured as the transient progresses. Cool down tests will follow a similar procedure. These tests were initiated.

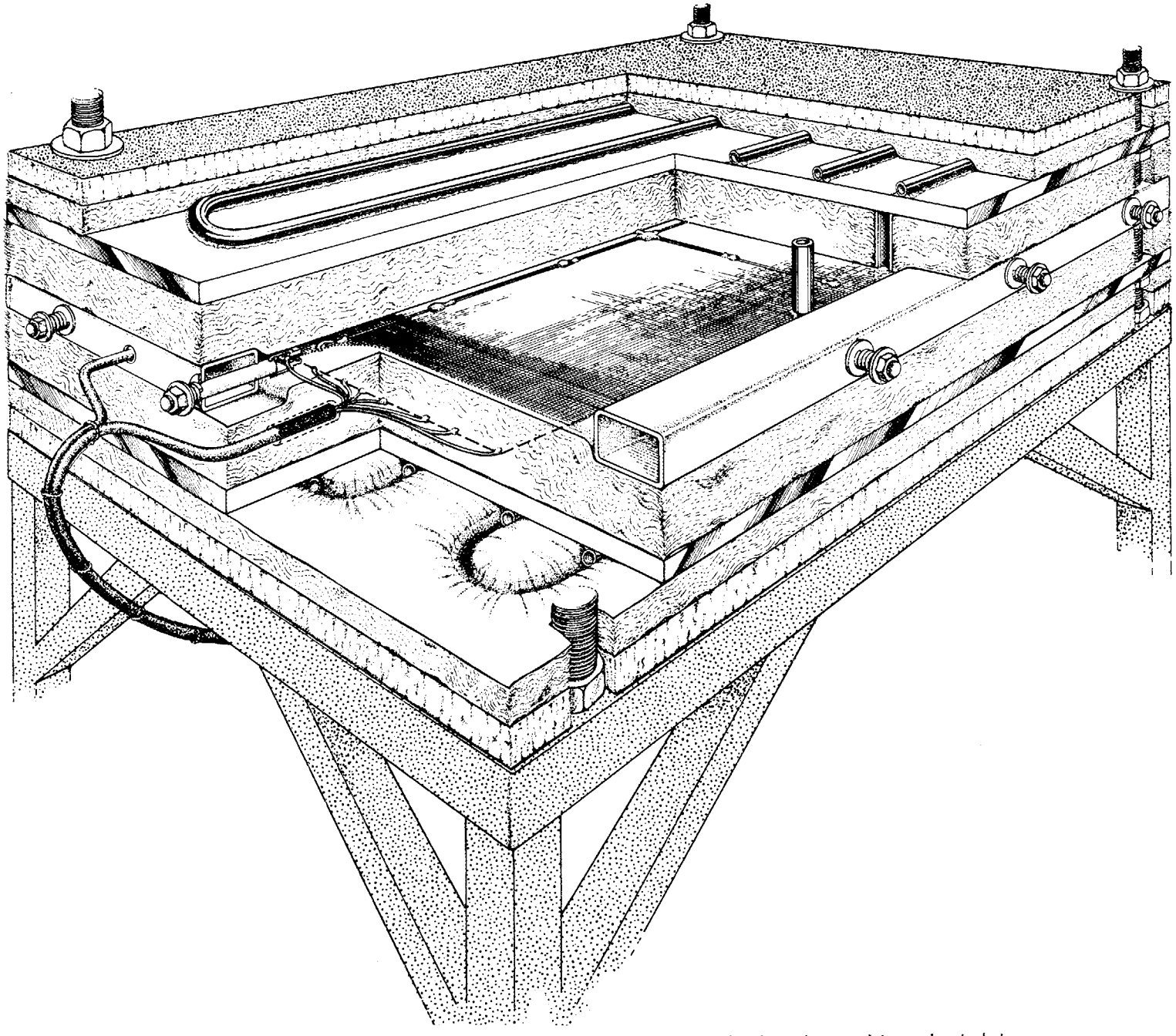

Fig. 23. Fixture for measuring thermal conductivity and developing thermal transient data.

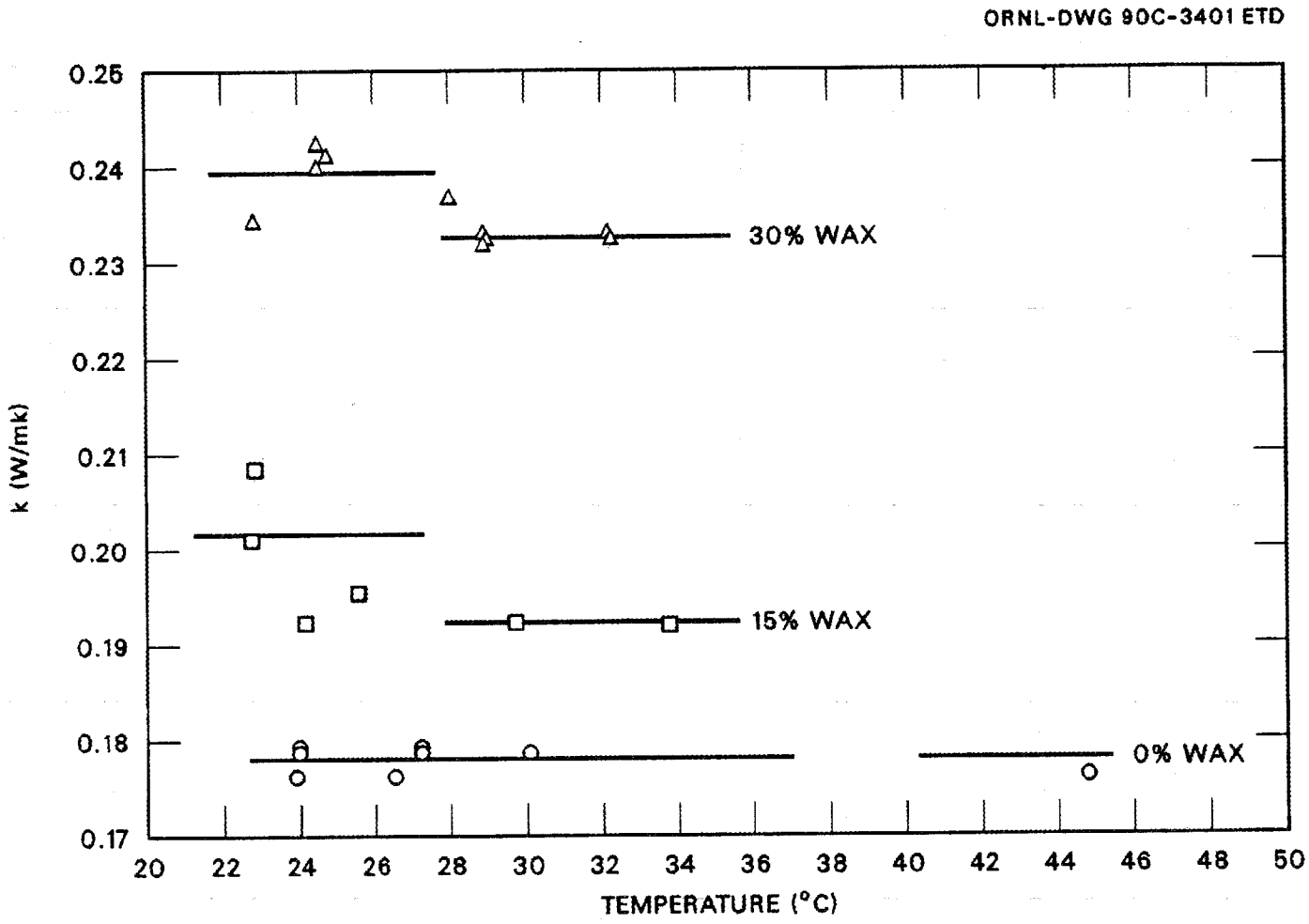

Fig. 24. Thermal conductivity as a function of temperature for gypsum-wax specimens.

3. TECHNICAL PROGRAM - INDUSTRIAL THERMAL ENERGY STORAGE

3.1 Packed Bed TES Model for Industrial Applications

Mississippi State University (MSU) has developed a computer model to describe thermal energy transport and storage in a packed bed of PCM materials. The model is directed toward high temperature storage for industrial applications such as the capture and reuse of heat from the high temperature flue gases. The governing mathematics of the model and many of the computational results were discussed in an earlier annual progress report.[12]

During this reporting period, a number of modifications were made in the model to enhance its capability for brick plant design optimization studies. These modifications are such that the model will be capable of handling the following:

1. A gas inlet stream to or from the packed bed with varying mass flow rates, temperatures, and chemical compositions specified by the user.

2. Gas-to-pellet radiation heat transfer and pellet-to-pellet conduction during periods of no flow.

3. As many as five different PCMs distributed vertically within the bed.

4. Thermal effects due to the packed bed containment vessel wall.

5. The effect of temperature-dependent properties of the inlet stream on heat transfer and pressure drop in the TES system.

The improved code was applied to regeneration of heat from the flue of a periodic brick-making plant. For this application, it was assumed that flue gas, which is normally exhausted from a plant, could be passed through a packed bed of PCM pellets that are layered according to phase change temperature to store heat. Following charging, the bed was

discharged cocurrently using outside air. The results from this study, as shown in Figs. 25-27, are for a packed bed utilizing five PCMs with phase-change temperatures of 1000K, 900K, 800K, 700K, and 500K. All other thermophysical properties (including the latent heat of fusion) for the different PCMs were assumed identical. The inlet gas, for both the charge and discharge cycle, was held at a constant temperature and flowrate. The results also include a dwell period when there was no flow through the bed. Figure 25 shows various bed temperatures as a function of dimensionless time ($\tau = \propto t/\ell^2$), where $\propto$, t and ℓ are thermal diffusivity, time and bed length, respectively. Figures 26 and 27 show the axial temperature profiles at various times for the charge and discharge cycle.

Figure 28 compares the fluid (gas) outlet temperature as a function of time for the following three cases:

1. One case corresponding to the transient response shown in Fig. 25 for a bed utilizing five PCMs.

2. A second case uses the five PCMs as before but assumes the containment vessel wall to be thermally isolated from the gas stream through the bed; i.e., this solution ignores the effect of the thermal mass of the containment vessel wall and the thermal conduction through it to the ambient air.

3. The third case includes a containment vessel wall effect but uses only one PCM with a phase-change temperature of 1000K.

It was noted that including the thermal response of the wall in the calculation has a significant effect on the results. In this case, the wall was assumed to be made of a thick ceramic material which adds considerable thermal mass to the packed bed.

Figures 29 and 30 are based on a hot gas temperature for charging the bed that increases with time. Figure 29 is for a packed bed utilizing a single PCM with a melting point of 1000K. Figure 30 is for a packed bed utilizing the PCM materials with melting points of 1000K, 900K,

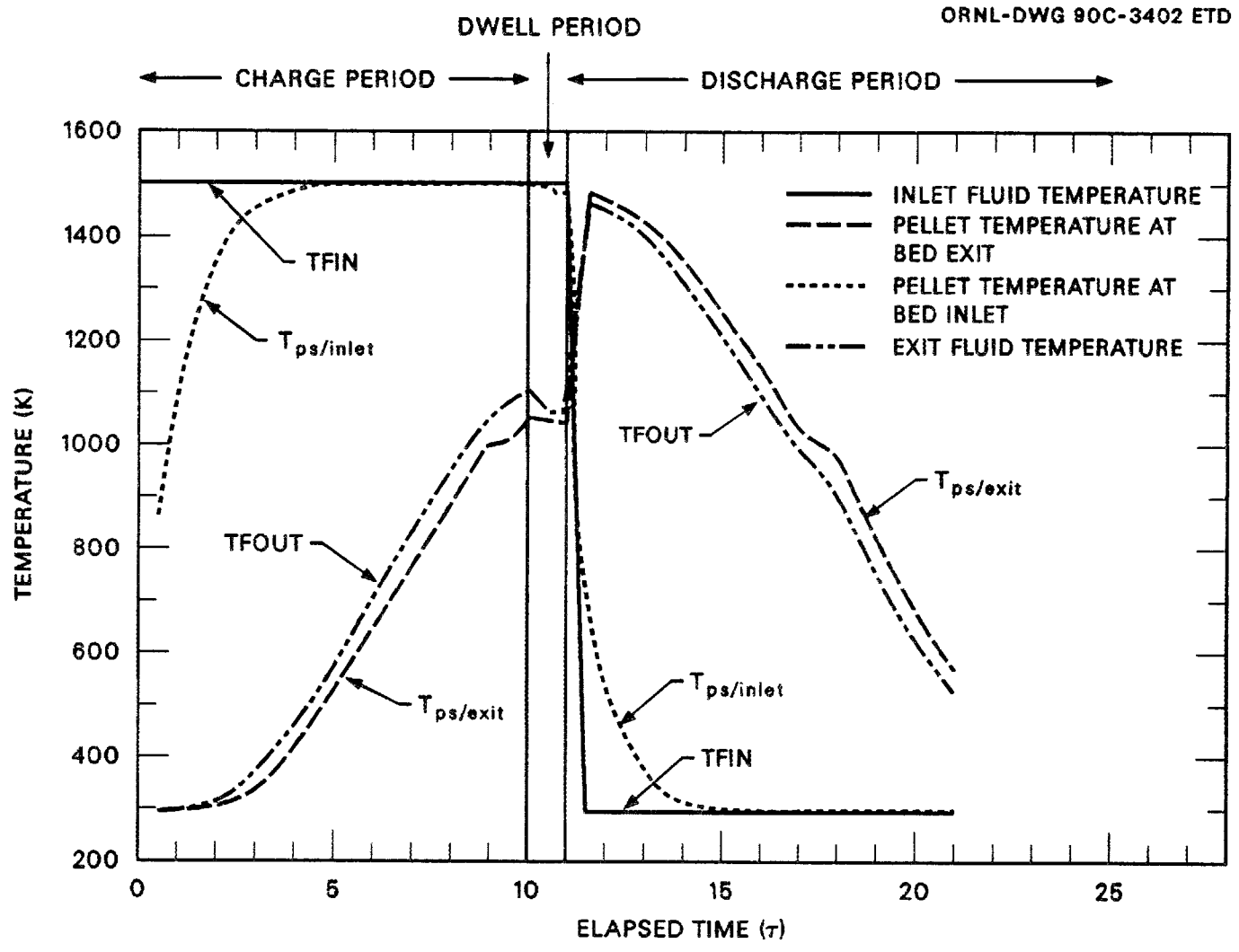

Fig. 25. Transient response over a complete cycle (charge, dwell, and discharge) for a packed bed utilizing five different PCMs; mass flowrate = 0.5 kg/s-m^2.

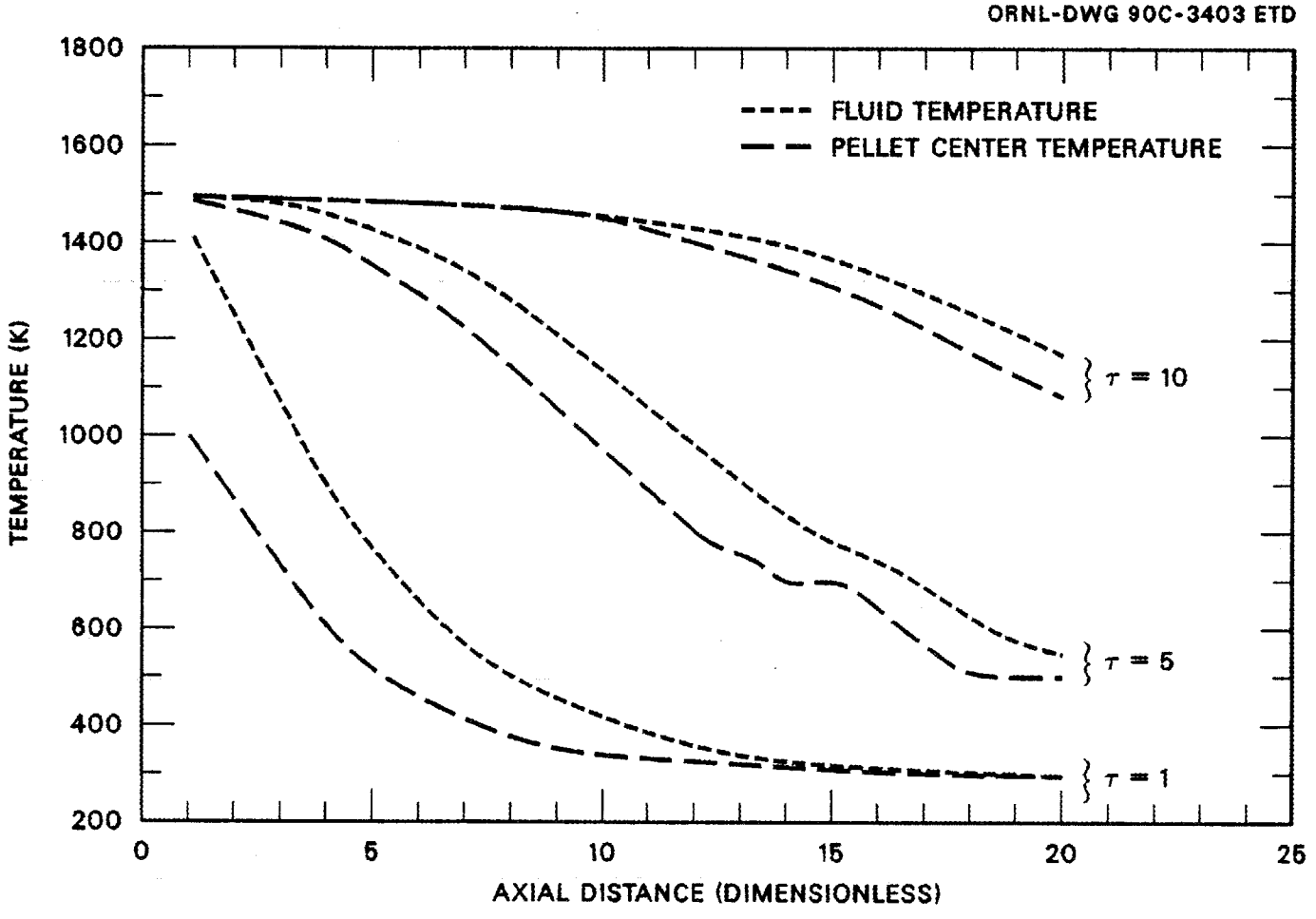

Fig. 26. Temperature-axial position profiles for a packed bed utilizing five families of PCM; charge period.

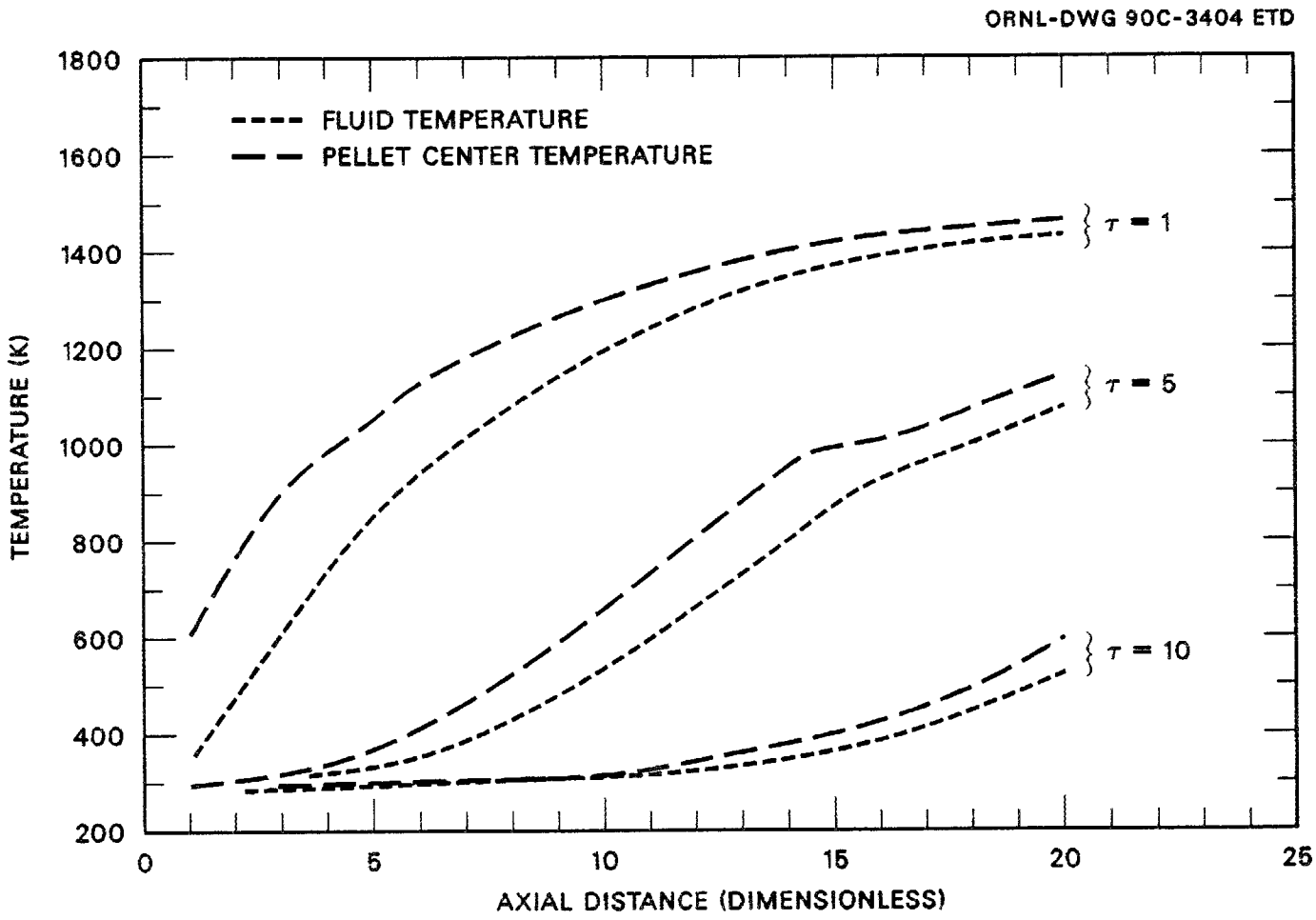

Fig. 27. Temperature-axial position profiles for a packed bed utilizing five families of PCM; discharge period.

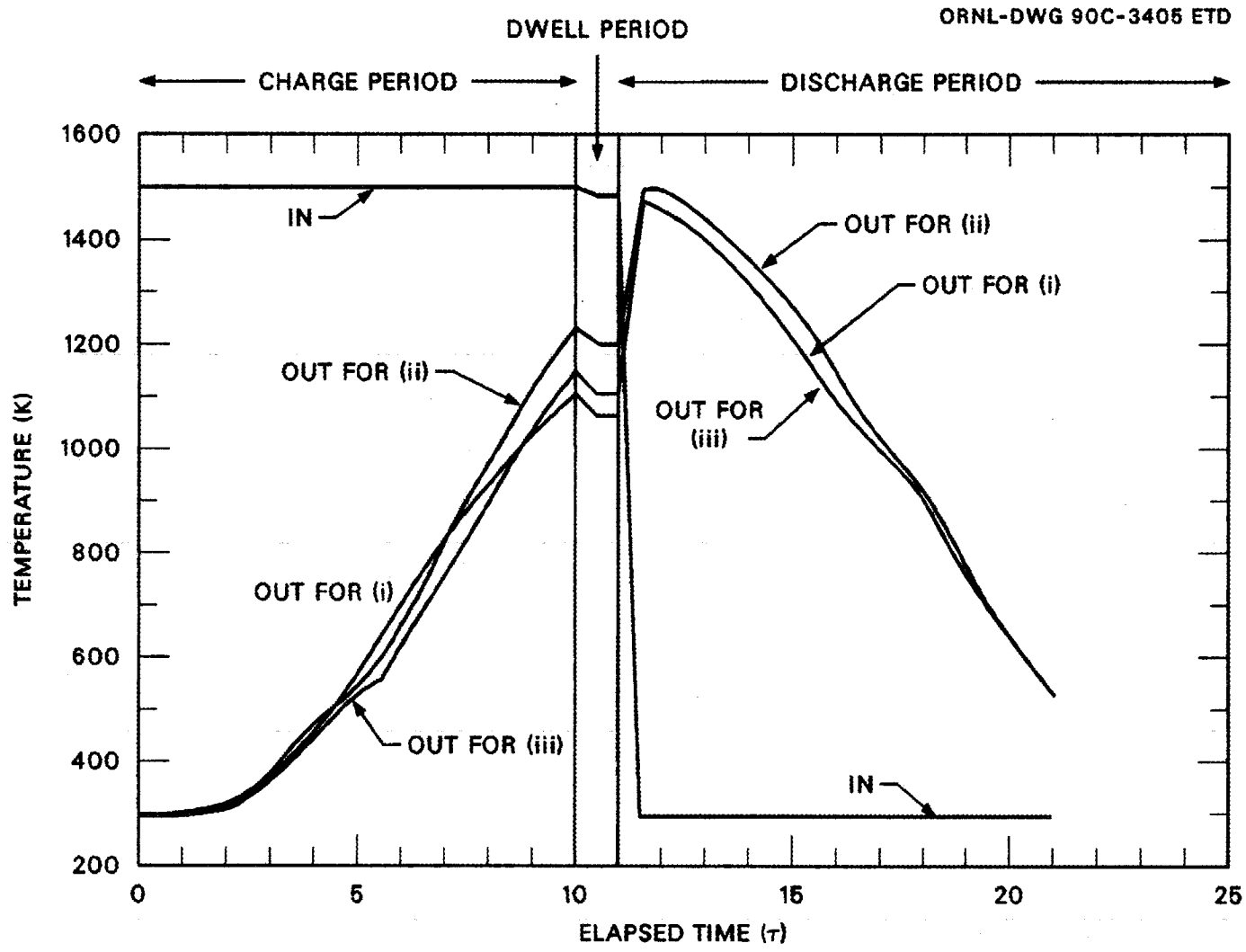

Fig. 28. Comparison of the transient performance for the packed bed: (i) utilizing five PCM sets, (ii) utilizing five PCM sets with wall effect neglected, and (iii) utilizing one PCM. IN = inlet fluid temperature; OUT = outlet fluid temperature.

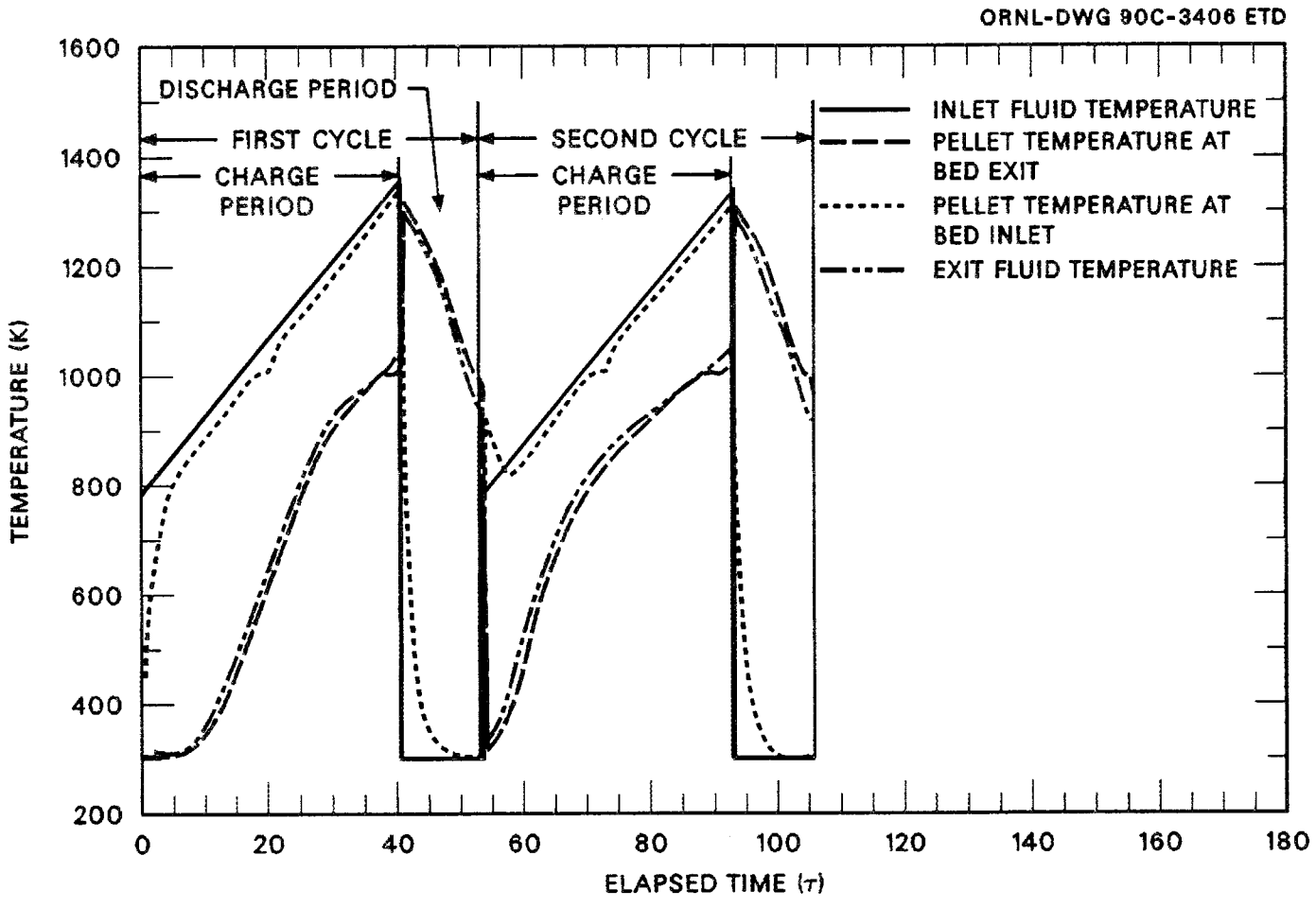

Fig. 29. Transient performance of the packed bed TES unit utilizing one PCM family; T_{ph} = 1,000K.

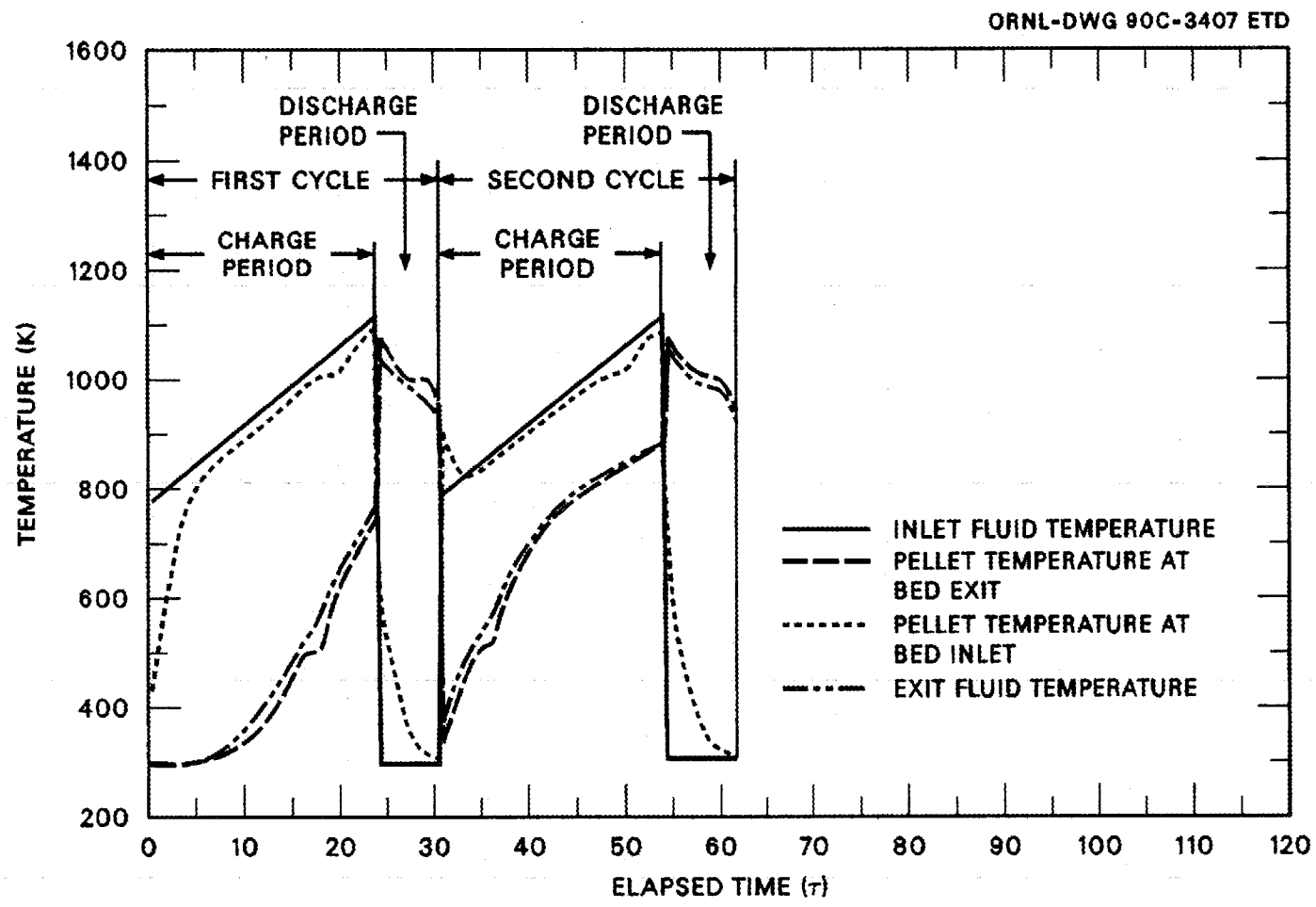

Fig. 30. Transient performance of the packed bed TES unit utilizing five PCM families; T_{ph} = 1,000K, 900K, 800K, 700K, and 500K.

800K, 700K, and 500K. All the figures show a relatively small temperature difference between the fluid and the pellet surface. The phase change process is evident as perturbations in the otherwise smooth pellet temperatures at ~1000K.

This research effort was directed toward developing the computer model and did not include any optimization studies for the packed bed. Nevertheless, sufficient runs were conducted so that some tentative conclusions can be reached:

1. The thermal mass of the packed bed containment wall is sufficiently great that it cannot be ignored in the design of a high temperature TES unit.

2. The performance of a bed packed with PCM pellets of different phase change temperatures placed as layers along the axis of the bed will be greater than a bed packed with pellets of a single melting point.

3.2 TES Optimization for Periodic Brick Plant

A previous study on the application of TES to periodic kilns in the brick, clay, ceramic, and refractory industry[13] identified three uses of stored heat that was extracted from the kiln flue gases: drying product greenware, preheating the ware prior to kiln firing, and pre-heating combustion air feeding the kiln burners. The study recommended a centrally-located TES unit that would store heat from the kiln for reuse to preheat combustion air for other kiln runs or to provide heat to the dryer. The need for storage is greatest when supplying the dryer because it requires less energy than the kiln but over a longer period of time. Rough estimates indicated that all the fuel used by the dryer might be eliminated by a well-designed TES system. Payback periods were estimated at two to four years.

Although the original study was not based on optimization principles, there are many aspects of the design and operation of a brick plant with TES that can be optimized which would improve the economic outlook for a TES system. To fill this need, development of a

computerized general optimization method was initiated to maximize the return-on-investment (ROI) for a brick plant capable of storing energy for use during periods when the kilns are not operating.

To fix ideas, a two-kiln periodic plant with a single dryer was considered. Figure 31 shows all possible connectors between the kilns, dryer, two heat exchangers (HE), and a TES unit, and Fig. 32 shows the operating schedule.

It is a common practice to recycle waste heat between simultaneously operating devices. Storage, however, opens the possibility of significantly expanding this capability. As can be seen in Fig. 32, if efficient redistribution of waste heat from kiln 1 and kiln 2 is possible, significant amounts of heat can be stored and made available for use by the dryer during week 1 and week 4, and kiln 2 during week 3.

A computer code, REUSE1, was developed which simulates all relevant aspects of the storage, heat transfer, and flue-gas-derived waste heat redistribution in the system. For the plant of Fig. 31, this involves 31 possible connections between devices, together with the addition of the heat exchangers and storage device. Also accounted for are the electricity costs involved in operating blowers for pumping the various gasses through the system, fuel costs, and valves for mixing various air and gas streams in the system. The system is optimized for maximum ROI over a typical operating cycle. Optimization is carried out in two stages: an "outer" stage, involving possible physical configurations of the system including ducts, pumps, etc.; and an "inner" stage involving redistribution of heated gasses. The outer loop optimization is carried out using top-down and bottom-up searches, while the inner loop is done via a simplex method (linear programming) approach, based on the linear system of constraints and conservation relations. Similarly, an inner "iteration" is carried out involving alternative iterations of temperatures in ducts and mass flow rates through them.

Three classes of independent variables affect the cost of the brick plant. First, are the geometric or configuration variables that specify which connections exist between devices. The second are operational variables which consist of the mass flow rates under control of the

ORNL-DWG 90-3408 ETD

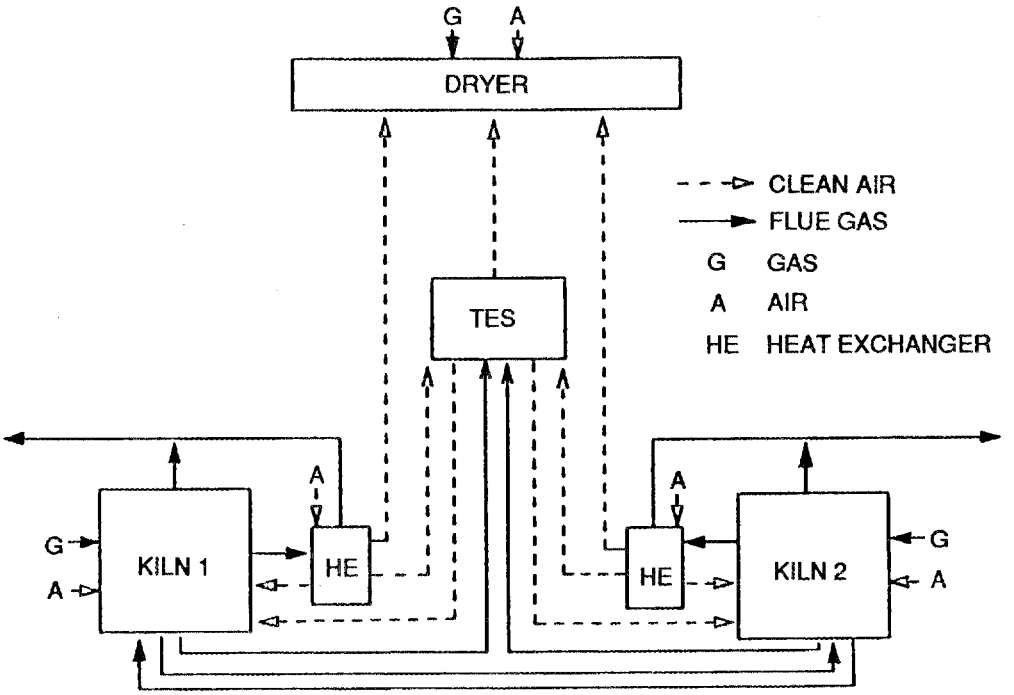

Fig. 31. Example brick plant.

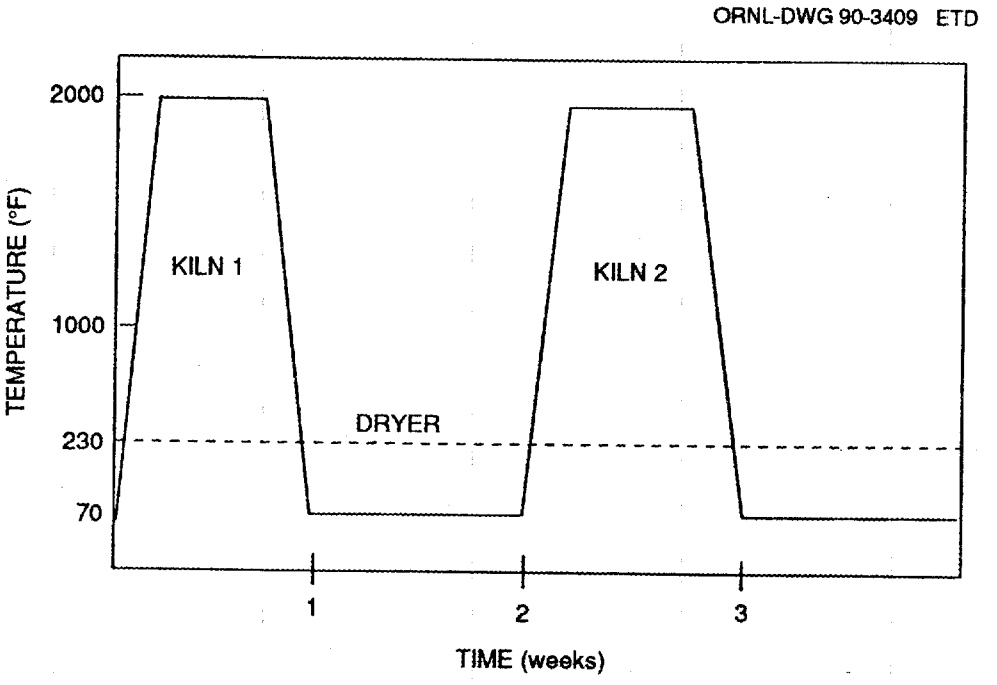

Fig. 32. Example plant schedule.

plant operator. The gas mass flow rate and the combustion air flow rates are determined by the burn requirements, and the flow rates of clean air directly into each device may be adjusted. By adjusting the flow rates, the amount of waste heat going into storage or into immediate use by a device can be controlled. The third class of independent variables are sizing and device variables. This class includes the size of the storage and the physical parameters that govern its performance, such as the melt temperature and specific heat of the PCM in the TES unit. The heat exchanger efficiency as a function of actual geometry or heat transfer coefficient is also in this class. The size of pipes and ducting between devices may also be considered in this class.

The primary impact of the operational variables is on the fuel costs, while the geometric variables impact the capital costs primarily. The sizing variables enter in a much more complicated fashion. In fact, many enter the cost function as nonlinear terms. For example, the size of the ducts affects the size of the fans and the cost of fan operation. The size of the pipes enters the cost function in both the capital and the operating portions. The size influences the electric requirements necessary for given mass flow rates.

Finding the optimal plant design and operation is the ultimate goal of the project. In pursuit of this goal, three layers of the optimization have been identified. First, the daily or hourly operation of the plant can be optimized with respect to operating costs. Second, the plant connections can be optimized to provide the maximum ROI for operation over a specified period. And third, the size and characteristics of each device can be optimized in the context of the optimal plant. These layers define optimization problems that must be done one within another.

The current work optimizes the first two layers simultaneously. This resembles certain operations research problems but has additional complications that make this problem unique and very difficult. The first complication is the time dependence of the mass flow rates. At each hour, or some appropriate time interval, the optimal mass flow rates must be found. With the addition of storage, the possibility exists for the instantaneous (1 hour interval) optimals to give no longer the optimal solution over the entire plant schedule.

Optimization without storage can be described as a search on connections and device sizes coupled with the simplex algorithm to optimize the time interval mass flow rates. The optimization of the first two layers is accomplished in the following steps:

Geometric Optimization

Downwards Search

1. Beginning with a fully connected plant, find the optimal mass flow rates for each time interval of the simulation.

2. Assign a cost to each link and remove the most costly connection to the lowest fuel consuming device.

Upwards Search

1. Beginning with an unconnected plant, find the energy costs of each device at each hour of the simulation.

2. Add one connection between the device having the highest cost and the source with the least connection cost.

Operational Optimization

Apply the simplex method, with constraints, to the plant at each hour of the simulation. For each configuration, we find the mass flow rate resulting in the least total operating cost.

With a TES unit included in the brick plant, the inner operational optimization is not necessarily the desired optimum. The operational optimization will always favor immediate reuse of heat to storage, since it has a limited time interval over which to optimize. With TES,

the future operation of the plant effects the optimal strategy for reuse of waste heat. Rather than immediate reuse of waste heat, it may be that storage to satisfy a thermal demand at a future time is more cost effective.

The time dependent storage problem resembles some inventory and production scheduling problems familiar to the operations research community. During the reporting period, a dynamic programming approach has been taken. The method can be described by considering a grid of time values and permissible TES states at each of these time points. For illustration, suppose that storage can be filled (by simply dumping excess heat at a prescribed rate) in increments of 1/4 of the TES unit's capacity. There are then five storage levels that the plant can have: empty, 1/4, 1/2, 3/4, and full. Since it is required that storage be filled or emptied during a time interval through one of these increments, then the other mass flow rates can be found optimally along with a cost associated with the plant operation over this time interval.

Suppose now that the cost of operation is given (computed by the simplex algorithm) for each point of the time-storage grid and for each possible increment of the state of the storage. This defines a directed graph with costs associated to each storage increment option. An example of such a graph is given in Fig. 33. The graph edges, a, b, c, d, and e, have costs associated with each of them. The dotted lines which move from less to more storage over the time interval indicate an infeasible solution. There is no heat available from the kiln during this period and, consequently, storage can only discharge. Each "x" in Fig. 33 would have similar edges and costs associated with possible storage paths.

To find the optimal schedule, the optimal path through this graph must be determined. A simple search technique was developed for this purpose. The search proceeds by finding the cheapest path from one of the first nodes to each node at a time level say i. To find the cheapest paths from this first node to each of the nodes at time level i+1 requires comparison of five paths for each of the five nodes. Upon arriving at the end of the network in this forward marching algorithm, the cheapest path from the first node to any ending node is known. In

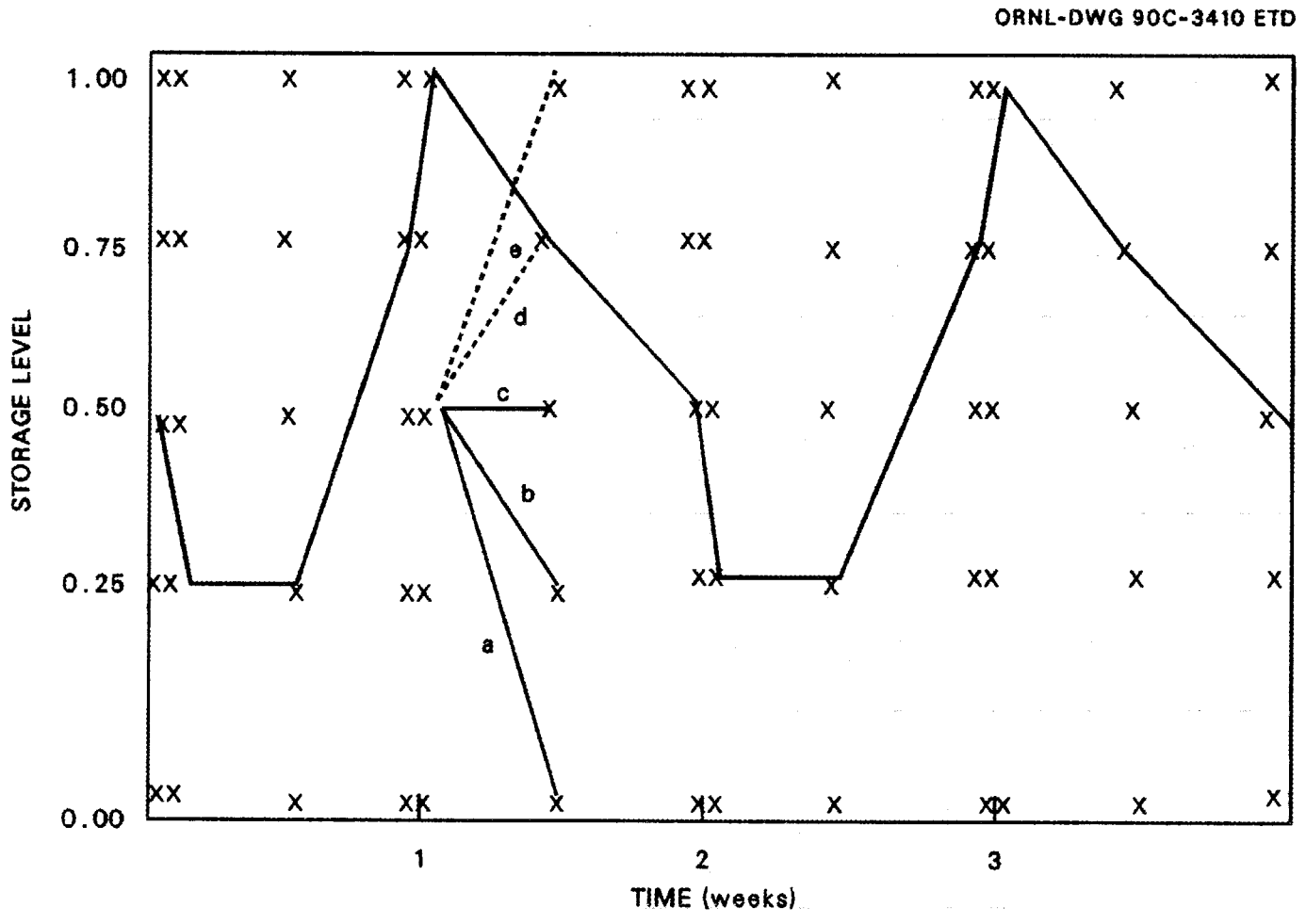

Fig. 33. Dynamic storage optimization.

Fig. 33, a periodic "optimal" path is shown, which would indicate the best use of storage. (This is an example and is not the result of any computation.)

The inclusion of TES and heat exchangers also requires that the temperatures be known for each connection in the network. Unfortunately, the temperatures interact non-linearly with the mass flow rates, so that they cannot be determined by the simplex algorithm. Some of the constraints coming from the devices are given in terms of maximum temperatures. To incorporate the temperature considerations, an iterative technique in which the best temperature guess is used to define constraints and costs for the simplex method was used. Once the mass flow rates which minimize the cost function are found, the temperatures of the network can be calculated. These newly-calculated temperatures are then fed back into the simplex method, and the mass flow rates are recalculated. This procedure repeats until convergence of the mass flow rates and temperatures is obtained.

The output from the computer program consists of return on investment values for each possible step of the dynamic programming algorithm. The periodic schedule that maximizes ROI for the duct configuration is found and output.

4. CONCLUSIONS

The diurnal and industrial TES program is continuing to show progress not only toward development of technologies but to their implementation as well. Each project is targeted to an application to facilitate transfer of the technology to industry. Of major emphasis for near-term technology transfer is development of a PCM wallboard; this goal is supported by a coordinated set of projects. This level of attention is commensurate with the potential market size for the product and interest shown by plasterboard manufacturers. In the low temperature area, the heat and mass transfer rate of dry bed reactors for ammoniated complex compounds was improved to the point that development of a cost-effective system seems within reach. Strong manufacturer interest has been shown in this technology as well; it is anticipated that further development of the chill storage system will proceed under a cost-shared arrangement.

The projects in the diurnal and industrial TES program form a strong basis for addressing energy-related issues that, through storage, can be successfully resolved. Work accomplished in the reporting period on these projects has produced results that will aid in this resolution.

REFERENCES

1. H. Hersh, "Ice-Building-A Sticky Problem," Paper No. 30, *Opportunities in Thermal Storage R&D*, EPRI/EM-3159-SR, Electric Power Research Institute, July 1983, pp. 30-1 and 30-2.

2. K. Itagaki, "Adhesion of Ice to Polymers and Other Surfaces," *Physiochem-Aspects Polym. Surf.* 1, 241-252 (1983).

3. H. H. G. Jellinek, "Adhesion of Ice Frozen from Dilute Electrolyte Solutions," *ACS Symp. Ser.* 8, 248-260 (1975).

4. W. E. Stewart, "Development of Improved Ice-Making Techniques for Storage Heat Pumps," *ASHRAE Trans.* 94 (2), 419-431 (1988).

5. E. B. Baumeister and C. O. Bennett, "Fluid-Particle Heat Transfer in Packed Beds," *AIChE J.* 4 (1), 69-74 (1958).

6. D. Chandra and C. Barrett, *Effect of Interlayer and Substitutional Dopants on the Thermophysical Properties of Solid-State Phase Change Materials*, Final report to the DOE, Contract No. DE-AC03-84SF12205, January 1986.

7. P. G. Grodzka, *Feasibility Study of Binary Solutions for Thermal Energy Storage in High and Low Temperature Applications*, ORNL/Sub/83-13858/1, Martin Marietta Energy Systems, Inc., Oak Ridge National Laboratory, December 1984.

8. J. J. Tomlinson and M. J. Taylor, *Thermal Energy Storage Technical Progress Report April 1986-March 1987*, ORNL/TM-10715, Martin Marietta Energy Systems, Inc., Oak Ridge National Laboratory, February 1988.

9. A. Solomon, V. Alexiades, D. Wilson, G. Geist, and J. Kerper, *An Enthalpy Method for the Solidification of a Supercooled Liquid*, ORNL/TM 6217, Martin Marietta Energy Systems, Inc., Oak Ridge National Laboratory, 1986.

10. C. Kohlenberger, *An Investigation into Low Temperature Thermal Energy Storage Technologies*, Kohlenberger Associates Consulting Engineers, Inc., Fullerton, California, September 1987.

11. I. O. Salyer and O. S. Duvall, "Passive Phase Change Materials for Use in Passive and Hybrid Solar Heating and Cooling Systems," *Proc. of the Passive and Hybrid Solar Energy Storage Update*, DOE/Conf.-8409118, U.S. Department of Energy, Washington, D.C., September 1984, pp. 61-71.

12. J. J. Tomlinson and R. J. Kedl, *Thermal Energy Storage Technical Progress Report April 1987-March 1988*, ORNL/TM-11233, Martin Marietta Energy Systems, Inc., Oak Ridge National Laboratory, September 1989.

13. "Thermal Energy Storage System Definition Study and Industry Characterization for the Brick, Clay, and Ceramic Industry," Institute of Gas Technology, Chicago, June 1982.

ORNL/TM-11492
Dist. Category UC-202

Internal Distribution

1. T. D. Anderson
2. D. W. Burton
3. R. S. Carlsmith
4. W. G. Craddick
5. J. B. Drake
6. D. M. Eissenberg
7. W. Fulkerson
8. J. A. Getsi
9. J. E. Jones Jr.
10. L. Jung
11. R. J. Kedl
12. M. A. Kuliasha
13. W. R. Mixon
14. F. R. Mynatt
15. M. Olszewski
16. A. E. Ruggles
17. A. C. Schaffhauser
18. M. Siman-Tov
19. T. K. Stovall
20. M. J. Taylor
21-25. J. J. Tomlinson
26. C. D. West
27. ORNL Patent Office
28. Central Research Library
29. Document Reference Section
30-31. Laboratory Records Department
32. Laboratory Records (RC)

External Distribution

33. Daniel M. Blake, Branch Manager Materials Research, Solar Energy Research Institute, 1617 Cole Boulevard, Golden, CO 80401
34. S.R. Bull, Solar Energy Research Institute, 1536 Cole Blvd., Golden CO 80401
35. Howard Coleman, Office of Solar Heat Technologies, U.S. Department of Energy, Forrestal Building, CE-314, 1000 Independence Avenue, Washington, DC 20585
36. Kevin Drost, Battelle Pacific Northwest Laboratories, P.O. Box 999, Battelle Boulevard, Richland, WA 99352
37. Russ Eaton, Office of Energy Storage and Distribution, U.S. Department of Energy, Forrestal Building, CE-32, 1000 Independence Avenue, Washington, DC 20585
38. Imre Gyuk, Office of Energy Storage and Distribution, U.S. Department of Energy, Forrestal Building, CE-32, 1000 Independence Avenue, Washington, DC 20585
39. Landis Kannberg, Battelle Pacific Northwest Laboratories, P.O. Box 999, Battelle Boulevard, Richland, WA 99352
40. Al Landgrebe, Office of Energy Storage and Distribution, U.S. Department of Energy, Forrestal Building, CE-32, 1000 Independence Avenue, Washington, DC 20585
41. George Manthey, DOE, Oak Ridge Operations, P.O. Box E, Oak Ridge, TN 37831
42. Allessio Mezzina, Brookhaven National Laboratory, Upton, NY 11973
43. Dave Pellish, U.S. Department of Energy, Forrestal Building, MS CE-332, Room 5H079, 1000 Independence Avenue, Washington, DC 20585
44. Veronika A. Rabl, Electric Power Research Institute, 3412 Hillview Avenue, P.O. Box 10412, Palo Alto, CA 94303
45. Eberhart Reimers, Office of Energy Storage and Distribution, U.S. Department of Energy, Forrestal Building, CE-32, 1000 Independence Avenue, Washington, DC 20585

46. Robert L. San Martin, Deputy Assistant Secretary of Renewable Energy, Department of Energy, CE-30, 6C-026/Forrestal Bldg., 1000 Independence Avenue, Washington, DC 20586
47. Office of Assistant Manager for Energy Research and Development, Department of Energy, ORO, Oak Ridge, TN 37831

48-160. Given distribution as shown in DOE/TIC-4500 under Category UC-202 (Thermal Energy Storage)